Article

Cell Reports

Visual Motion Processing in Macaque V2

Graphical Abstract

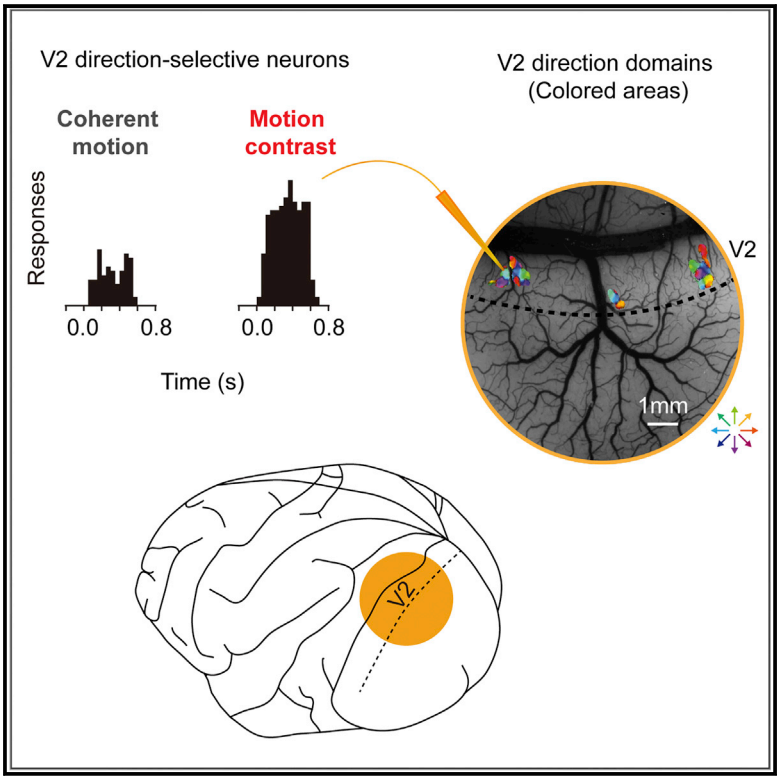

Authors

Jiaming Hu, Heng Ma, Shude Zhu, ..., Xingya Cai, Kun Yan, Haidong D. Lu

Correspondence

haidong@bnu.edu.cn

In Brief

Direction-selective (DS) neurons are widely distributed in the primate visual system. Hu et al. examined visual responses of DS neurons in the second largest visual area (V2) in macaque monkeys and demonstrate distinctive response properties of these neurons compared with DS neurons in the well-studied traditional motion area MT.

Highlights

- DS neurons in a non-dorsal visual area (V2) were studied with map-guided recordings
- V2 DS neurons exhibit features distinct from the DS neurons in the dorsal area MT
- Clusters of V2 DS neurons form functional architectures sensitive to motion contrast
- Response properties of V2 DS neurons are suitable for figure-ground segregation

Hu et al., 2018, Cell Reports *25*, 157–167
October 2, 2018 © 2018 The Author(s).
https://doi.org/10.1016/j.celrep.2018.09.014

CellPress

Cell Reports
Article

OPEN ACCESS
CellPress

Visual Motion Processing in Macaque V2

Jiaming Hu,[1,2,3] Heng Ma,[2] Shude Zhu,[1,2] Peichao Li,[1,2] Haoran Xu,[1,2] Yang Fang,[1,2] Ming Chen,[1,2] Chao Han,[1,2] Chen Fang,[2] Xingya Cai,[2] Kun Yan,[2] and Haidong D. Lu[2,3,4,*]
[1]Institute of Neuroscience, Chinese Academy of Sciences, and University of Chinese Academy of Sciences, Shanghai 200031, China
[2]State Key Laboratory of Cognitive Neuroscience and Learning, IDG/McGovern Institute for Brain Research, Beijing Normal University, Beijing 100875, China
[3]Interdisciplinary Institute of Neuroscience and Technology, Qiushi Academy for Advanced Studies, Zhejiang University, Hangzhou 310027, China
[4]Lead Contact
*Correspondence: haidong@bnu.edu.cn
https://doi.org/10.1016/j.celrep.2018.09.014

SUMMARY

In the primate visual system, direction-selective (DS) neurons are critical for visual motion perception. While DS neurons in the dorsal visual pathway have been well characterized, the response properties of DS neurons in other major visual areas are largely unexplored. Recent optical imaging studies in monkey visual cortex area 2 (V2) revealed clusters of DS neurons. This imaging method facilitates targeted recordings from these neurons. Using optical imaging and single-cell recording, we characterized detailed response properties of DS neurons in macaque V2. Compared with DS neurons in the dorsal areas (e.g., middle temporal area [MT]), V2 DS neurons have a smaller receptive field and a stronger antagonistic surround. They do not code speed or plaid motion but are sensitive to motion contrast. Our results suggest that V2 DS neurons play an important role in figure-ground segregation. The clusters of V2 DS neurons are likely specialized functional systems for detecting motion contrast.

INTRODUCTION

One of the fundamental functions of visual systems is to measure and use visual motion signals to maintain continuity of perception of the constantly changing environment. Neurons that particularly signal the visual motion direction are pervasive among different species (Mauss et al., 2017). Such neurons were first found in primary visual cortex of cat by David Hubel (Hubel, 1959) and then discovered in many other mammalian species, including primates (Hubel and Wiesel, 1968). In primates, research on visual motion processing has been focused on the dorsal visual stream (V1-MT-MST), among which middle temporal area (MT) has been extensively studied (Born and Bradley, 2005).

More recently, imaging studies in humans and monkeys suggest that analysis of visual motion is a distributed process, which involves many areas such as areas V2 and V4, in addition to the traditional motion areas in the dorsal stream (Orban et al., 2003). However, the response features of DS neurons outside of dorsal areas and their functional roles in motion processing are still largely unexplored. As the second largest visual area in the monkey brain, area V2 plays important roles in processing contour, color, and depth information (Sincich and Horton, 2005). However, its functional role in motion processing is relatively unclear. V2 contains ~17.5% DS neurons (Figure 1), which preferentially locate in the thick stripes (Levitt et al., 1994; Shipp and Zeki, 2002) and cluster to form functional maps (Lu et al., 2010). Considering the large size of V2 (comparable to V1 and ~10 times the size of MT, [Felleman and Van Essen, 1991], also see Figure 1), the number of DS neurons in V2 and MT should be at least comparable, which means that V2 DS neurons encode a large amount of motion information beyond the traditional V1-MT motion pathway.

Relative motion among different objects in the visual scene can be used as a salient cue for inferring the structural information (motion parallax). It has been shown that V2 is involved in orientation detection of the boundaries formed from relative motion (motion/kinetic boundary) (Chen et al., 2016; Marcar et al., 2000; Peterhans and von der Heydt, 1993). This kind of boundary helps a figure to pop out from its background. Previously, it was suggested that V2 may convey motion information from V1 to MT (V1-V2 thick stripes-MT); however, recent cooling studies have shown that this pathway may contribute primarily to binocular depth perception and little to motion (Ponce et al., 2008, 2011; Smolyanskaya et al., 2015). Although DS neurons in V2 and MT both receive inputs from V1, they likely receive inputs from different types of V1 neurons (Nassi et al., 2006; Nassi and Callaway, 2007) and thus may have different response properties and functional roles. So far, whether and how V2 DS neurons play a role in motion-related object detection remains unknown.

To characterize the selectivity of V2 neurons and have a better understanding of their features, we examined response properties of DS neurons with map-guided single-cell recordings. We found that the majority of these neurons had a small receptive field (RF) size and were weak in motion integration and speed detection. However, these neurons had a strong antagonistic surround and preferred motion contrast. Besides, the high concentration of these motion contrast sensitive neurons in V2 indicates an anatomic architecture focusing on handling motion contrast signals, which may contribute to figure-ground segregation.

This is an open access article under the CC BY-NC-ND license (http://creativecommons.org/licenses/by-nc-nd/4.0/).

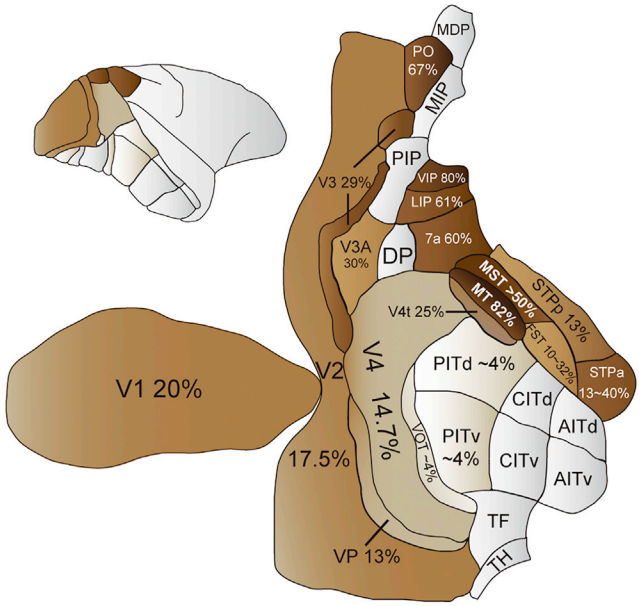

Figure 1. Percentages of Direction-Selective Neurons in the Monkey Visual Cortex

A flattened visual cortex map with percentages of direction-selective (DS) neurons labeled for each area. References for the percentage values are listed in Table S1. The visual cortex map is modified from Figure 2 in (Felleman and Van Essen, 1991, with permission). Only visual areas are shown here. Areas containing a higher proportion of DS neurons are shown in darker colors. Areas with unknown percentages (no recording data) are shown in gray. Although dorsal areas have higher percentages of DS neurons, there are significant proportions of DS neurons in ventral areas (e.g., V4) and non-dorsal areas (e.g., V2). See also Table S1.

RESULTS

For each case (hemisphere), a chronic chamber was implanted, which permits both optical imaging and single-cell extracellular recordings. Data were collected from 9 hemispheres of 8 rhesus monkeys under anesthesia. A total 254 single neurons were investigated, of which 203 were from V2 direction domains and 51 from V2 regions away from direction domains.

V2 Direction Maps

Consistent with previous reports (Lu et al., 2010), clusters of direction domains were observed in all 9 cases. Figures 2B–2D show example functional maps obtained from one case. Each map is a t-map that compares images collected in two different stimulus conditions (illustrated at the bottom). The border between areas V1 and V2 (dotted line) was determined by ocular dominance imaging (Figure 2B). Figures 2C and 2D show two motion direction maps, each obtained by comparing responses to random dots (RDs) drifting in 2 opposite directions. Clusters of direction domains (indicated by white arrows) were observed only in area V2, not in V1, consistent with our previous study (Lu et al., 2010). The mean diameter of single direction-preference domains was 279.6 ± 69.8 μm (mean ± SD, n = 102, same convention below). The coverage of V2 direction domains, as estimated from direction maps, was approximately 8.5% ± 3.1% (n = 7) of the total V2 surface imaged.

Map-Guided Single-Cell Recordings

In electrophysiological experiments, the locations of the V2 direction domains were drawn on the surface blood vessel maps to guide the placement of electrode penetrations (Figure 2E).

Figure 2F shows the raster plots of an example neuron's responses to gratings drifting in 12 directions. This neuron exhibited a clear direction preference with a direction index (DI) value of 1.01. For neurons recorded in V2 direction domains (n = 203), their DI distribution was unimodal (Figure 2G), with a high mean DI value (0.79 ± 0.31). This indicates that most neurons recorded in the direction domains were DS neurons. Furthermore, these neurons also responded well to moving RDs and exhibited similar directional preference as to moving gratings (Figure S2). We used DI >0.67 as the classification criteria for DS neurons (Levitt et al., 1994) and determined that 70.4% (143/203) neurons recorded from V2 direction domains are DS neurons. Detailed RF properties of these V2 DS neurons are listed in Table S2. We also observed that, within one penetration, there was a tendency for DS neurons to have similar preferred directions. Large shifts in the preferred direction were only observed occasionally (Figures S1K–S1N), thus DS neurons were organized into direction columns in V2. Penetrations were also made targeting V2 regions away from the direction domains (mostly orientation domains). Very few DS neurons were observed (only 1/51) in these non-direction domain recordings. The DI distribution of these 51 neurons is shown as an inset in Figure 2G for comparison.

Suppressive RF Surround

To examine neurons' center-surround structure, we first mapped neurons' CRF (classical receptive field) with a small patch of drifting gratings. An example of the RF is shown in Figure S1J, which revealed the overall shape of the RF and the RF center location (strongest response location). Then, in an area summation test, a circular patch of grating was presented at various sizes centered at the neuron's RF center. Size tuning curves of 2 example neurons are shown in Figure 3B. Cell 1 exhibited only weak surround suppression as its responses reached a plateau as the stimulus size increased. Cell 2 had strong surround suppression and did not respond to large stimuli at all. Almost all V2 DS neurons tested showed a certain degree of surround suppression, and most of them decreased their responses more than half when responding to large stimuli (i.e., surround suppression index >50; Figure 3C, upper panel). The mean surround suppression index value of V2 DS neurons (71.4 ± 25.1, median = 74.2) was much larger than that of non-DS neurons recorded either inside or outside the direction domains (51.4 ± 32.5, p = 0.0033, Wilcoxon test; Figure 3C, lower panel). This value was also larger than the values measured from MT neurons (median = 35, Pack et al., 2005; median = 63, Raiguel et al., 1995). In addition, unlike in MT (Born, 2000; Born and Tootell, 1992), no "reinforcing surround" neurons were observed in our V2 recordings. Mean surround suppression of V2 DS neurons was also stronger than those reported for V1 neurons

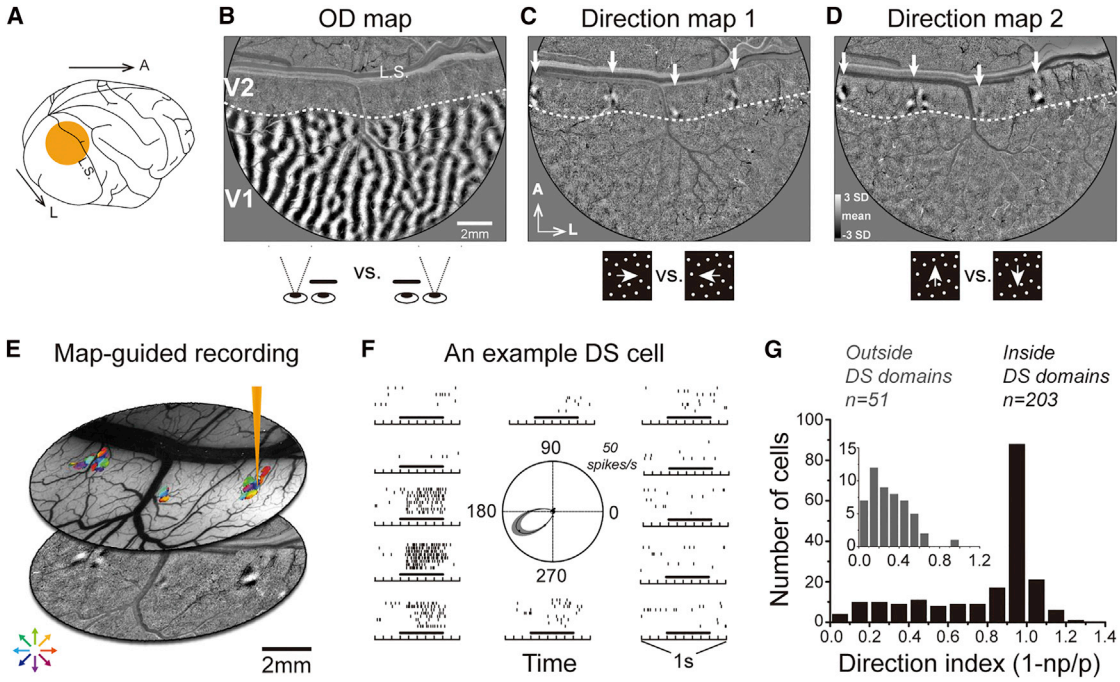

Figure 2. V2 Direction Maps and Map-Guided Single-Cell Recordings

(A) A schematic of the macaque brain with imaging region indicated (brown disk). L.S., lunate sulcus.

(B–D) Functional maps (t-maps) obtained with optical imaging from an example case (case 1).

(B) An ocular dominance map in V1. The V1/V2 border is indicated by a dotted white line.

(C) A "right vs. left" direction map obtained by comparing responses to random dots moving in opposite directions. Direction domains (white arrows) are clustered in restricted regions in V2. Note that the anterior part of V2 is folded into the lunate sulcus which underlies the large blood vessel on the top.

(D) Similar to (C), an "up vs. down" direction map obtained by comparing responses to upward and downward moving random dots. Clusters of direction domains are found in the same locations as in (C) (white arrows).

(E) An illustration of map-guided single-cell recordings. V2 direction domains were drawn on a surface blood vessel map. Different colors indicate different direction preferences of these direction domains.

(F) An example neuron recorded from a V2 direction domain. Raster plots show the neuron's responses to gratings drifting in 12 directions. Short horizontal bars indicate the stimulus presentation time (0.5 s). The gray region around the tuning function represents ± 1 SEM.

(G) Distribution of direction indexes (DI) of 203 neurons recorded in 79 penetrations targeting V2 direction domains from 8 monkeys. DI is calculated as 1-np/p, in which p and np are the responses to preferred and anti-preferred directions. Most neurons recorded (143/203, 70.4%) showed strong direction selectivity (DI >0.67). The inset plot shows the DI distribution obtained from 51 neurons recorded outside the direction domains (in 19 penetrations from 6 monkeys). The vast majority of neurons recorded outside direction domains are not direction-selective (DI <0.67).

See also Figures S1 and S2.

(Sceniak et al., 2001): 0.88 (V2) versus 0.63 (V1) when calculated with a different of Guassian (DOG) model fitting method.

The RF size, defined as the optimal patch size in the area summation test was 1.17° ± 0.82° for V2 DS neurons (Figure 3D), which was smaller than that of MT neurons (4°–17°, Felleman and Kaas, 1984) at comparable eccentricities. V2 DS neurons' RF sizes were also relatively smaller than those of V2 non-DS neurons recorded (1.62° ± 1.43°), but such a difference was not statistically significant (p = 0.24, Kolmogorov-Smirnov test).

Independent Spatial-Temporal Tuning and Insensitivity to Pattern Motion

Neurons' SF and temporal frequency (TF) tuning features were measured with drifting sine-wave gratings (Figures S3C and S3D). On average, V2 DS neurons had a preferred SF of 2.16 ± 2.81 cycle/degree, and a preferred TF of 8.29 ± 3.86 Hz. In a spatial-temporal dependency test, only 3 out of 68 V2 DS neurons fitted well with the speed-tuning model, while the majority neurons were either unclassed (20/68) or better fitted with the independent model (45/68). This is very different from the neurons recorded from MT where much more speed-tuned neurons were found (Figure S3F; Priebe et al., 2003). The independent spatial-temporal tunings indicate that these neurons are not speed tuned.

We also tested whether V2 DS neurons showed selectivity to pattern motion, which was observed in many MT neurons (Movshon et al., 1985). The stimuli were drifting plaids similar to those used in MT recordings (Smith et al., 2005). Among the 59 tested V2 DS neurons, only 8.5% (5/59) showed significant plaid motion selectivity (Figure S4B), while this percentage in MT is 25% (Smith et al., 2005; Figure S4C).

Sensitivity to Motion Contrast

To measure neurons' responses to motion contrast within their RF centers, we used stimuli that contained two sets of RDs, each moved coherently (transparent motion, Figures 4A and

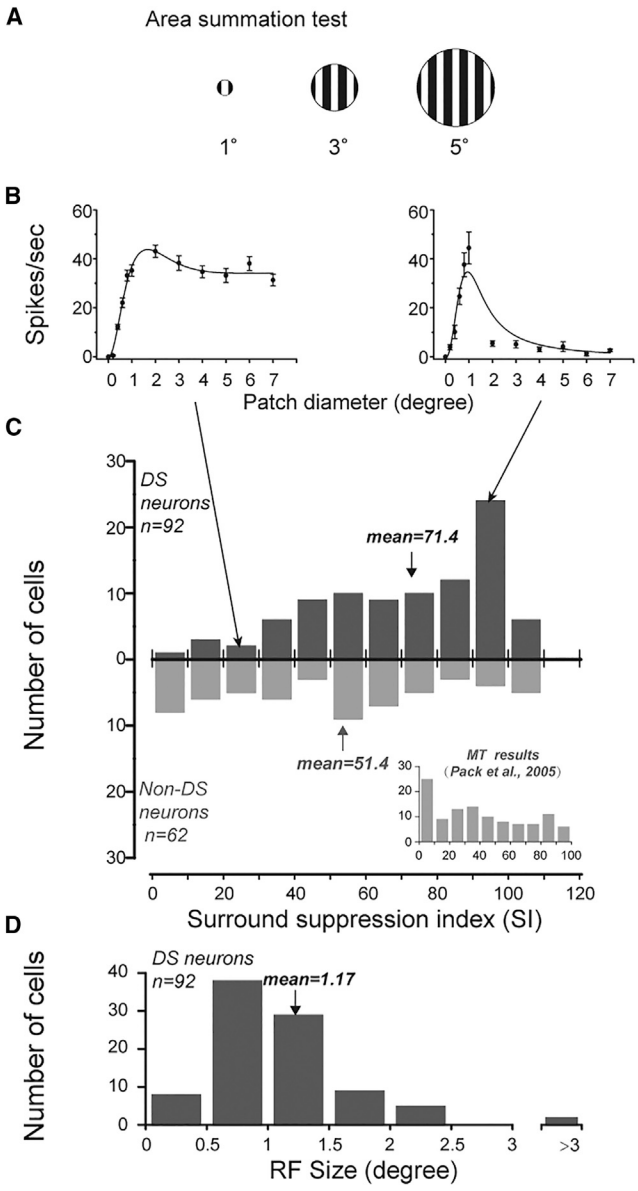

Figure 3. V2 DS Neurons Have Strong Surround Modulation

(A) Illustrations of visual stimuli for the area summation test. The gratings were drifting at the neuron's preferred direction. Gratings were used here since both DS neurons and non-DS (such as orientation-selective) neurons were tested.

(B) Size tuning curves of 2 example neurons in the area summation test. They showed weak (left) or strong (right) surround suppression when the stimulus size was increased beyond their classical RF. Error bars ± SEM.

(C) Distribution of surround suppression index (SI) of DS neurons (top, 92 neurons from 6 monkeys) and non-DS neurons (bottom, 62 neurons from 6 monkeys), as calculated from the area summation test: SI = 100 × (1-R7/Rmax). DS neurons showed greater surround suppression (mean = 71.4) than non-DS neurons (mean = 51.4, p = 0.0033, Wilcoxon test). Inset plot shows the SI distribution of MT neurons (adapted from Figure 1B in Pack et al., 2005, with permission).

(D) Distribution of V2 DS neurons' RF sizes as measured from the fitting curves in the area summation test.

4B). These results indicate that within the RF centers, the responses of V2 DS neurons were suppressed when non-optimal motions were added into the existing optimal motion stimuli, a feature similar to MT neurons but different from their input V1 neurons (Qian and Andersen, 1994; Snowden et al., 1991).

We also tested how surround motion modulates neurons' responses (surround direction test, Figures 4D–4F). In 53 tested V2 DS neurons, 43 (81%) neurons showed strong surround modulation (modulation index >0.5), similar to the example shown in the right panel of Figure 4E. Responses were weaker when the center and surround moved in the same direction, compared with the responses to the opposite center-surround motion condition. The mean modulation index (MI) value of these 43 neurons was 81.4 ± 15.8, which means that, on average, these neurons' responses to large motion stimuli were suppressed by 81.4% compared with their responses to the optimal stimulus (opposite center-surround motion). The rest 19% of neurons (10/53) did not show strong modulation by the surround direction (left-panel example in Figure 4E), and their mean MI value was 6.3 ± 49.6. There was a positive correlation between the MI value and SI value (Figure S5, r = 0.47, p = 0.0004, Spearman test). In the recordings of 31 of these 53 neurons, we added an additional stimulus condition in which only center dots moved and the surround dots kept stationary (center-alone condition). For 22.6% (7/31) of the tested neurons, their responses to opposite surround motion even exceeded their responses to the center-alone stimulus. Thus, these neurons had a two-way surround modulation, depending on the surround motion direction: either suppressive (for uniform center-surround motion) or facilitative (for opposite center-surround motion).

The RF structure of V2 DS neurons is summarized in Figure 4G. It is similar to the "double-opponent" model that has been described previously for cat area 17 neurons (Palmer and Naf-ziger, 2002). The "double-opponent" neurons are supposed to be more sensitive to "contrast" than simple center-surround antagonistic neurons. It should be noted that for the majority of the recorded V2 DS neurons, anti-preferred motion in their RF surrounds only had a lower degree of suppression (compared with the suppression caused by surround motion in the preferred direction), only 22.6% neurons exhibited a facilitation effect (a true "double-opponent"). Besides, many DS neurons we recorded did not have a perfect symmetric suppressive surround. But overall, the degree of asymmetry was not high (Figure S6C).

Sensitivity to Motion Boundary Locations

For most of V2 DS neurons, they possessed a clear antagonistic center-surround structure (Figure 4G). Neurons with such a RF feature are suppressed by large field stimuli but may be less suppressed when their RF is stimulated by a motion boundary (MB) at an appropriate location. To test this directly, we investigated how neurons responded to a single MB presented at different positions near and inside their RFs. Figures 5B and 5C show an example V2 DS neuron's responses to horizontal MB stimuli. In the 2 different configurations of stimuli (Ha and Hb), the strongest responses were observed when the MB was placed at the edge of its CRF (position 0.5° in Figure 5B and position −0.5° in Figure 5C). In these two optimal response conditions, the RF center was stimulated by its preferred motion (red arrows), while a portion of its surround

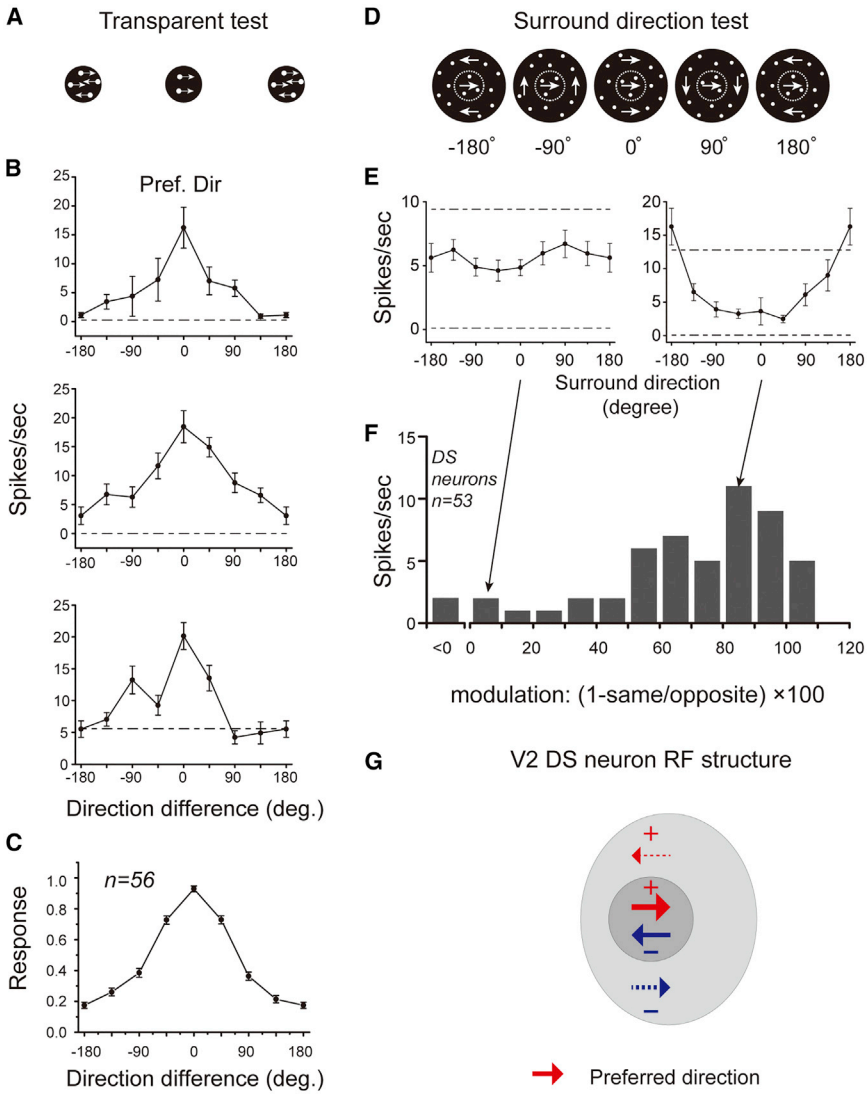

Figure 4. Responses to Motion Contrast

(A) Illustration of the visual stimuli for transparent test. Two sets of RDs covered the RF center; each drifted coherently. One set of RDs drifted in the neuron's preferred direction; the other set drifted in various of directions.

(B) Responses of 3 example neurons to the transparent motion. x axis shows the angle difference between the non-preferred RD direction and the preferred RD direction (0°). Error bars ± SEM.

(C) Population results (56 neurons from 5 monkeys) of the transparent motion test. Error bars ± SEM.

(D) Illustration of the visual stimuli used to test the surround modulation. The RF center was always stimulated with dots moving in the neuron's preferred direction. The RF surround was stimulated with an annular RD patch where the directions of RDs were varied from trial to trial (8 direction conditions), including the neuron's preferred direction (0°).

(E) Responses of 2 example DS neurons to the surround direction test. Dashed lines: responses to center patch only (top) and spontaneous level (bottom). Error bars ± SEM.

(F) Distribution of the surround modulation index [(1-same/opposite) × 100] of the tested V2 DS neurons (53 neurons from 6 monkeys).

(G) Illustrations of the antagonistic center-surround RF structure of V2 DS neurons. When only the CRF is stimulated, a DS neuron responds best to its preferred direction and is inhibited by the opposite direction. Outside this CRF, there is a large RF surround. The neuron does not respond when its surround is stimulated alone. The stimulation of the RF surround can modulate the neuron's responses when the center is also stimulated. The "preferred" surround direction is opposite to the center one. Different thicknesses of the arrows indicate different strengths of the modulation effects.

See also Figures S5 and S6.

was stimulated by dots moving in its anti-preferred direction. In these two particular conditions, the neuron's responses were stronger than that when a uniform motion RD pattern was presented and moving in the neuron's preferred direction (Figures 5D and 5E). Similarly, strongest responses were observed when MBs were placed off the RF center in vertical MB conditions. Figures 5F and 5G show this example neuron's tuning curves to different MB positions. In each panel, there are two curves corresponding to two sets of conditions in which motion directions in the two RD patches were switched. For both horizontal and vertical MB conditions, response curves peaked at the positions off the RF center, mostly at either −0.5° or 0.5° positions. As the RF size of V2 DS neurons was approximately 1°, the optimal response conditions were when the MBs were located at the edge of the RF. A summary of neurons' responses to MBs in different positions is presented in Figure S7.

For almost all V2 DS neurons recorded, their responses to uniform motions were weaker than their responses to the MB stimuli as the MB was placed at the appropriate positions (Figures 5F and 5G). Figure 5H shows that the peak responses in MB tuning curves (illustrated in Figures 5F and 5G) are larger than the neurons' responses to a uniform motion moving in their preferred directions. We calculated a modulation index (1-Rpre/Rmax, Rpre is the response to uniform motion moving in the neuron's preferred direction, Rmax is the average of maximum responses to Ha, Hb, Va, and Vb, Figures 5F and 5G) for such influence due to the existence of a MB. Most (42/43, 97.7%) of the modulation indexes were greater than 0, indicating an enhanced response over the uniform motion condition. This index was also positively correlated with the surround suppression index obtained in area summation test (Figure 5I).

Population Responses to MB

Thus far, most V2 DS neurons preferred visual stimuli containing motion contrast, and such a preference was due to their strong antagonistic surround modulations. Considering that V2 DS

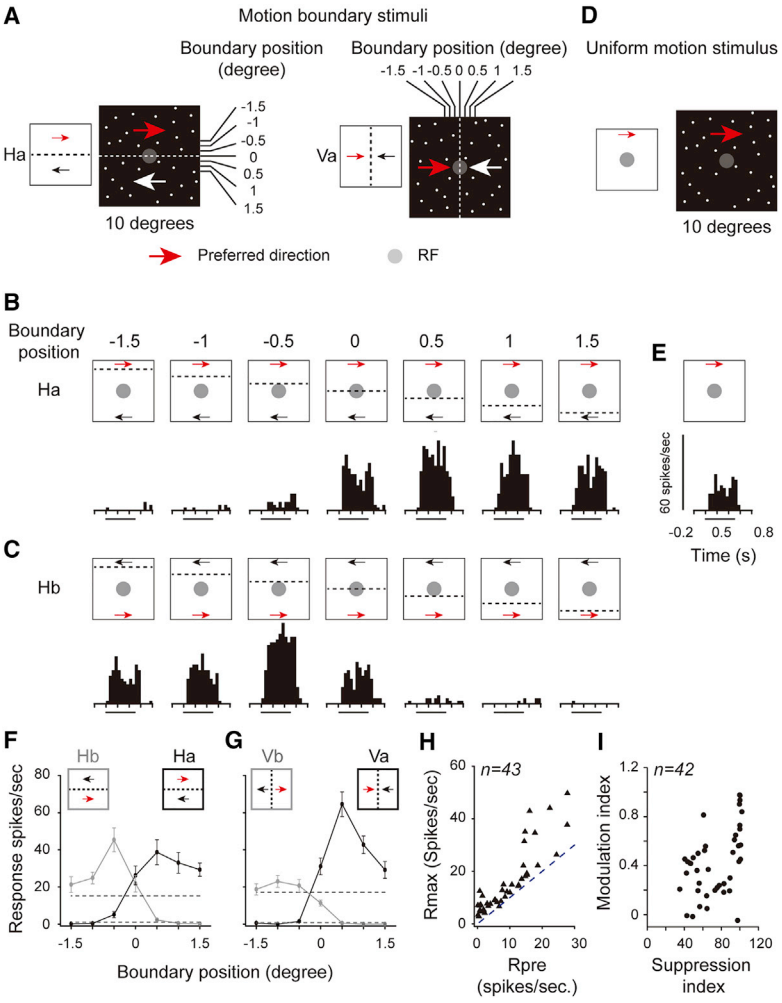

Figure 5. Modulation of DS Neurons' Responses by the Location of Motion Contrast

(A) Illustrations of horizontal (left) and vertical (right) MB stimuli. In each stimulus, two RD patches moved in opposite directions: one in the neuron's preferred direction (red arrow) and the other in the opposite direction (white arrow). The boundary between the two RD patches was placed at 7 different positions (conditions), separated by 0.5°. In condition 0, the MB was placed at the center of the RF (gray disk). "Ha" denotes type "a" horizontal MB conditions, while in "Hb" conditions, the two RD motion directions were switched (see C). Similar labels are used for "Va" and "Vb" stimuli.

(B) Responses of an example DS neuron to 7 horizontal MB conditions. Horizontal dotted lines represent different positions where the MB is placed relative to the RF (gray disk). Response histograms are shown under each stimulus. Short horizontal bars indicate the stimulus presentation time (0.5 s).

(C) Similar to (B), responses of the same neuron to MB conditions where two RD directions were switched.

(D) Illustrations of a uniform motion stimulus. The stimulus was similar to the MB stimuli in (A), except that all dots were moving uniformly in the neuron's preferred direction.

(E) The response histograms of the same example neuron in (B) and (C) to uniform RD motion.

(F) MB position tuning curves of the example neuron. Curve values were obtained from the response histograms shown in (B) and (C). The top dotted line represents the response level of the neuron to preferred uniform RD motion (E). The bottom dotted line represents the spontaneous level of the neuron. Error bars ± SEM.

(G) Similar to (F), position tuning curves for vertical MB conditions. Error bars ± SEM.

(H) Peak responses in MB tuning curves (y axis) were mostly larger than the neurons' responses to a uniform RD moving in their preferred direction (x axis) ($p < 0.001$, Wilcoxon test).

(I) Correlation of surround suppression index (from Figure 3C) and modulation index measured in the above MB test (from H: 1-Rpre/Rmax). These two indexes were positively correlated ($r = 0.51$, $p = 0.00057$, Spearman test).

See also Figure S7.

neurons had stronger suppressive surround than neighboring non-DS neurons, such a difference should be reflected in population responses in optical imaging. That is, V2 direction domains would show stronger responses to motion contrast stimuli compared to their neighboring V2 regions. To show that, we used stimuli containing multiple strips of RDs in which dots moved in opposite directions (Figure 6A, left, also see Video S1). The opposite motion of the RDs created strong motion direction contrast and a salient strip percept. The control stimuli (Figure 6A, right, also see Video S2) also contained strips of moving dots, but all dots were moving in the same direction, resulting in no motion direction contrast. We observed patches of strong differential activation (Figure 6B) in locations where DS neurons clustered (Figure 6C); such activation was not observed in V1 or other regions in V2. Thus, at population level, V2 DS neurons also exhibited preference to stimuli containing motion contrast.

As a summary, the RF features of V2 DS neurons we measured are listed in Table S2. RF features of V1 and MT DS neurons from previous studies are also listed. Detailed comparisons can be found in Discussion.

DISCUSSION

The most characteristic feature of V2 DS neurons is their strong surround modulation, which makes them suppressed by large field motion and activated by motion contrast. Unlike MT neurons, V2 DS neurons have a small RF and show little motion integration. Taken together, these properties make them more suitable for segregating a moving object from its background than detecting the object motion. The co-localization of direction domains and motion contrast sensitive areas in V2 suggests that V2 has developed specific functional architectures to deal with the motion contrast signals in the visual scene.

V2 DS Neurons: Compared with V1 DS Neurons

V1 and V2 contain similar proportions of DS neurons (V1: ~20%, V2: 17.5%, Figure 1, Table S1), and DS neurons in V2 likely inherit directional selectivity from their V1 inputs (Nassi and Callaway, 2007; Nassi et al., 2006; El-Shamayleh et al., 2013). Similar to V1 DS neurons, V2 DS neurons prefer a low SF (2.16 cycle/degree) and a relatively high TF (8.29 Hz). In contrast to V1,

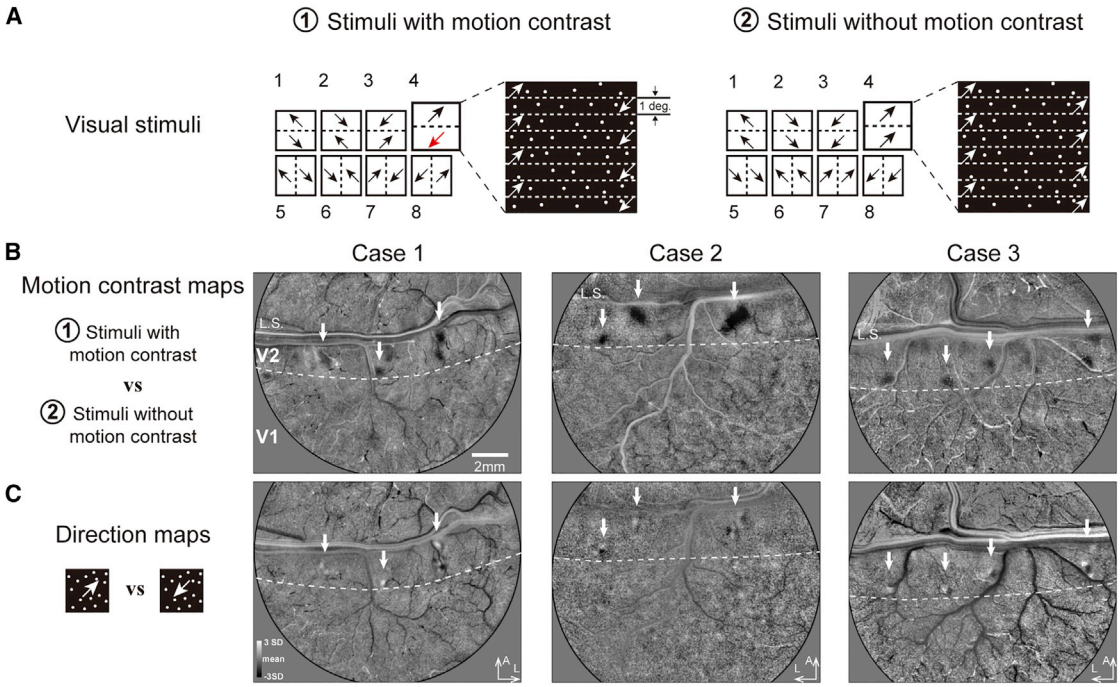

Figure 6. V2 DS Domains Were Strongly Activated by Motion Contrast

(A) Two sets of visual stimuli that either contain motion contrast (1) or not (2). Motion contrast was created by opposite directions of motion in neighboring RD strips (1). For stimuli without motion contrast (2), the dots are all drifting in the same direction while still appearing or disappearing at the virtual boundaries.

(B) Optical imaging of motion contrast maps that compare responses to stimuli (1) with responses to stimuli (2). Three cases are listed in three columns. Dotted lines represent the V1/V2 borders. Some regions in V2 (white arrows) were more activated by the stimuli with motion contrast (1) than those without (2). Other V2 regions and V1 did not show such a bias. L.S., lunate sulcus.

(C) Direction maps of the same 3 cases obtained by comparing RDs drifting in opposite directions. V2 direction domains co-localize with those regions that show motion contrast preferences (white arrows).

where DS neurons do not form iso-directional functional columns, V2 DS neurons cluster together and form a direction map (Lu et al., 2010 and this study). In our recordings (eccentricity 1°–5°), V2 DS neurons have a small RF size (1.17°), which is only slightly larger than the average of V1 neurons at the same eccentricity (~1°, Foster et al., 1985; Jones et al., 2001) and smaller than that of V1 complex DS neurons (1.8°, Bair and Movshon, 2004). In addition, speed tuning properties of V2 DS neurons (Figure S3) are more like V1 simple cells, not complex cells (Priebe et al., 2006). Thus, V2 DS neurons may selectively receive inputs from small RF, non-speed tuning V1 DS neurons. A small RF size indicates that only limited spatial integration occurs in these V1-V2 projections. In addition, the strong surround suppression in V2 DS neurons may further limit their ability in spatial integration.

A major difference between DS neurons in V1 and V2 is how they respond to transparent motion inside their RF. V1 DS neurons do not strongly attenuate when another set of RDs moving in a non-preferred direction is added into its preferred motion stimulus (Qian and Andersen, 1994; Snowden et al., 1991). However, responses in V2 DS neurons are remarkably attenuated by this type of transparent motion (Figure 4). This feature can potentially increase the sensitivity to motion contrast location (Figure 5) (compared with neurons without a transparent motion suppression).

It has been shown that neurons in V1 already have strong surround suppression and their responses can be modulated by motion directions outside the CRF (Lamme, 1995; Jones et al., 2001; Sceniak et al., 2001). Thus, strong surround suppression in V2 DS neurons (SI = 71.4, Figure 3C) seems inherited from their V1 inputs. However, at population level, V2 neurons have stronger surround suppression than V1 neurons (Zhang et al., 2005). Our analysis also shows that V2 DS neurons exhibit stronger surround suppression than V1 neurons reported in Sceniak et al. (2001). Furthermore, in our imaging results, V2 DS neurons are preferentially activated by stimuli containing motion contrast while such a response enhancement is not observed in V1 (Figure 6B). Thus, beyond the input from V1 neurons, there may be other mechanisms that strengthen the surround modulation of V2 DS neurons.

V2 DS Neurons: Compared with MT Neurons

There are a number of common features for V2 DS neurons and MT neurons. Both exhibit suppression by transparent motion when their CRFs are stimulated. In terms of surround suppression, about half of the MT neurons act like V2 DS neurons and have a suppressive surround (Born, 2000) and also exhibit tuning to MB location (Marcar et al., 1995). However, these two groups of neurons are significantly different (see below), which may coincide with previous findings that they receive different

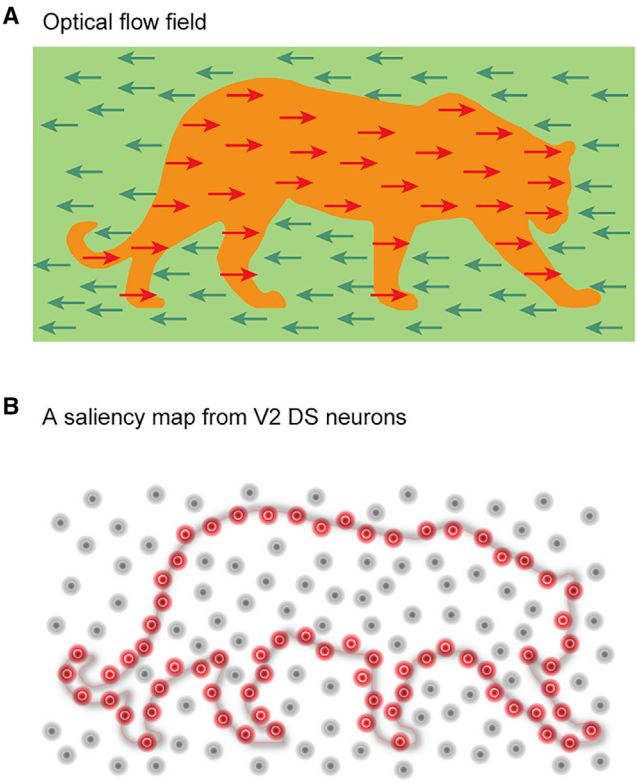

Figure 7. Illustration of a Salience Map Based on V2 DS Neurons' Responses to Motion Contrast

(A) The movement of a cheetah creates an optical flow field which separates this cheetah and its background (different colors).

(B) Small circular patches represent the RFs of V2 DS neurons. V2 DS neurons that have their RFs along the outline will enhance their responses due to the existence of motion contrast, while neurons that have their RF inside the outline or on the background will not show such strong enhancement. The outline of the cheetah thus can be detected based on such a spatial response pattern (a saliency map) created by a population of V2 DS neurons.

types of inputs (Gur et al., 2005; Gur and Snodderly, 2007; Nassi and Callaway, 2007; Nassi et al., 2006; Sincich and Horton, 2003).

One important difference is the size of their RFs. Our V2 DS samples were mainly from eccentricity 1°–5°. At this eccentricity, the mean RF size of MT neurons is approximately 4–5 times larger (Albright and Desimone, 1987), indicating a much greater spatial integration. One advantage of a small RF is to maintain the spatial information (location) about the optimal stimuli (e.g., the location of a MB).

Another difference between V2 and MT DS neurons is their RF surrounds. In MT, there are at least 2 types of surrounds, namely, antagonistic (suppressive) and reinforcing. Neurons with different RF surrounds spatially segregate in MT and form a columnar organization (Born and Tootell, 1992; Born 2000). In strong contrast to MT neurons, no reinforcing surround are found in V2 DS neurons, most of which either have an antagonistic surround (43/53) or exhibit no/weak surround direction tuning (10/53).

In addition, DS neurons in V2 and MT are also different in their responses to motion. Particularly, compared with MT neurons, V2 DS neurons are weaker in speed tuning and less sensitivity to plaid motion. These features suggest that, unlike in MT, motion analysis in V2 may not be optimized for detecting the motion signals per se. Instead, one of the important roles V2 DS neurons perform is likely detecting the motion contrast, along with its spatial locations in the dynamic visual scene (Figures 5 and S7). In summary, the differences between V2 and MT DS neurons appear more significant than their commonalities. The different strategies they take may eventually lead to completely different contributions to visual perception.

Motion-Based Object Detection

Humans and other mammals are capable of using different types of visual cues in detecting objects from their backgrounds. One of these cues is relative motion (Regan, 1986, 1989). For object detection, motion cues become critical when the other cues are confusing or not available, for example, in identifying a camouflaged insect. It has been shown that motion is one of the most efficient cues for shape perception (compared with cues of disparity, texture, density, etc., see Nawrot et al., 1996), and humans' abilities to detect the spatial properties of MBs are as precise as those for luminance boundaries (Regan, 1989; Regan and Hamstra, 1992).

Figure 7 illustrates a potential mechanism by which V2 DS neurons contribute to figure-ground segregation, which was originally proposed for MT neurons (Allman et al., 1985; Tadin and Lappin, 2005). During object motion, the optical flow at object boundaries often has strong motion contrast signals (Figure 7A). Those V2 DS neurons that have their RFs located near such motion boundaries will be strongly activated, while neurons that have their RFs located entirely within the object or the background will be suppressed (similar to conditions in Figures 5B and 5C). Thus, these activated V2 DS neurons form a saliency map for the object outline (Figure 7B). Readouts of this map can serve figure-ground segregation as well as shape analysis. For example, such outline information can be used to strengthen the interior responses which represent a "figure" (Lamme, 1995; Lamme et al., 1998). In addition, V2/V4 orientation neurons may receive information directly or indirectly from these activated DS neurons and detect boundary orientations (Chen et al., 2016) used for shape analysis. Marcar et al. (2000) reported about 11.5% V2 neurons are selective to MB orientations, but with a longer latency compared with their response to luminance boundaries. Based on this observation, they suggested that these neurons might receive feedback from higher-level areas (V4) where more MB-selective neurons were found. Another possibility is that the longer latency is due to local processes to integrate spatial information from motion contrast neurons in direction columns. The direct functional connections between DS neurons and MB selective neurons still need to be established.

Although many MT neurons also have a suppressive surround and can code precise MB locations at a population level (Chen et al., 2015), V2 DS neurons have the advantage of smaller RFs and stronger surround modulations (thus less dependent on population coding). V2 also appear to have a greater number of such neurons. These individual neuron properties suggest

that V2 DS neurons may be better candidates suitable for the task of MB detection.

Extracting object information from motion also fits the major role of V2 in visual processing. Unlike V1, V2 contains neurons that are selective to edge orientations defined by various types of visual cues, such as illusory contours (von der Heydt et al., 1984), stereoscopic contours (von der Heydt et al., 2000), and motion contours (Marcar et al., 2000; Chen et al., 2016). Why does the visual system develop such a cue-invariant contour detection in V2? One hypothesis is that such a basic function needs to be performed as early (and as fast) as possible (Hildreth and Koch, 1987) so that various types of contour information can be integrated into downstream object analysis.

Mounting evidence shows that visual motion processing in the primate brain is a distributed process and is not limited to the dorsal stream (Orban et al., 2003). Additionally, different motion stimuli or tasks activate different areas (e.g., Vanduffel et al., 2001). Thus, different functions tend to be supported by different neural circuits and processing strategies. It has been proposed that there are two fundamental types of motion processing strategies: integration and differentiation (Braddick 1993). These two types require different computational operations (additive versus differential), and likely being accomplished by different neurons with distinct RF properties. It has been shown that the motion integration process is achieved in the dorsal pathway, where pattern motion is detected (Movshon et al., 1985). Our present results suggest that the motion differential process is maintained and probably emphasized in the V1-V2 motion pathway. Meanwhile the "double-opponent" type of motion detection is developed.

Beyond V2, there are also large numbers of DS neurons in other areas whose functional roles are mostly unexplored (Table S1). In some areas, DS neurons also cluster and form direction maps (e.g., Li et al., 2013). This rich motion information may eventually contribute to many higher-order functions, e.g., shape-from-motion, biological motion, action understanding, and global motion. The exact strategies of motion processing can also be very different for different functions (and areas).

STAR★METHODS

Detailed methods are provided in the online version of this paper and include the following:

- KEY RESOURCES TABLE
- CONTACT FOR REAGENT AND RESOURCE SHARING
- EXPERIMENTAL MODEL AND SUBJECT DETAILS
- METHOD DETAILS
  - Intrinsic signal optical imaging
  - Map-guided single-cell recordings
  - Visual stimuli for optical imaging
  - Visual stimuli for single-cell recording
  - Electrophysiological data analysis
- QUANTIFICATION AND STATISTICAL ANALYSIS

SUPPLEMENTAL INFORMATION

Supplemental Information includes seven figures, two tables, and three videos and can be found with this article online at https://doi.org/10.1016/j.celrep.2018.09.014.

ACKNOWLEDGMENTS

This work was supported by the National Natural Science Foundation of China (31530029, 31625012, and 31371111) and the Hundred Talent Program of the Chinese Academy of Sciences. We thank Anna W. Roe for critical comments on the manuscript. Lab members J. Lu, J.W. Pan, J.J. Cai, C. Xu, and Z. Yu provided valuable technical assistance.

AUTHOR CONTRIBUTIONS

J.H. and H.D.L. conceived and designed the project. J.H. and H.M. performed most of the experiments. J.H. and S.Z. designed the electrophysiology recording setups. P.L., H.X., Y.F., M.C., C.H., C.F., X.C., and K.Y. advised on experimental design and helped the experiments. J.H. and H.D.L. wrote the manuscript with contributions from all other authors.

DECLARATION OF INTERESTS

The authors declare no competing interests.

Received: October 12, 2016
Revised: July 5, 2018
Accepted: September 6, 2018
Published: October 2, 2018

SUPPORTING CITATIONS

The following references appear in the Supplemental Information: Baizer et al. (1977); Baizer (1982); Bruce et al. (1981); Burkhalter and Van Essen (1986); Colby et al. (1993); Desimone and Ungerleider (1986); Desimone and Schein (1987); DeYoe and Van Essen (1985); Fanini and Assad (2009); Felleman and Van Essen (1987); Ferrera et al. (1994); Galletti et al. (1991); Gegenfurtner et al. (1996); Gegenfurtner et al. (1997); Hawken et al. (1988); Maunsell and Van Essen (1983); Mendoza-Halliday et al. (2014); Mikami et al. (1986); Miura et al. (2014); Mountcastle et al. (1987); Nowak et al. (1995); Orban et al. (1986); Orban (1996); Perge et al. (2005); Raiguel et al. (1999); Rosenberg et al. (2008); Siegel and Read (1997); Tamura et al. (1996); Tanaka et al. (1986); Van Essen and Zeki (1978).

REFERENCES

Albright, T.D. (1984). Direction and orientation selectivity of neurons in visual area MT of the macaque. J. Neurophysiol. *52*, 1106–1130.

Albright, T.D., and Desimone, R. (1987). Local precision of visuotopic organization in the middle temporal area (MT) of the macaque. Exp. Brain Res. *65*, 582–592.

Allman, J., Miezin, F., and McGuinness, E. (1985). Direction- and velocity-specific responses from beyond the classical receptive field in the middle temporal visual area (MT). Perception *14*, 105–126.

Arieli, A., Grinvald, A., and Slovin, H. (2002). Dural substitute for long-term imaging of cortical activity in behaving monkeys and its clinical implications. J. Neurosci. Methods. *114*, 119–133.

Bair, W., and Movshon, J.A. (2004). Adaptive temporal integration of motion in direction-selective neurons in macaque visual cortex. J. Neurosci. *24*, 7305–7323.

Baizer, J.S. (1982). Receptive field properties of V3 neurons in monkey. Invest. Ophthalmol. Vis. Sci. *23*, 87–95.

Baizer, J.S., Robinson, D.L., and Dow, B.M. (1977). Visual responses of area 18 neurons in awake, behaving monkey. J. Neurophysiol. *40*, 1024–1037.

Born, R.T. (2000). Center-surround interactions in the middle temporal visual area of the owl monkey. J. Neurophysiol. *84*, 2658–2669.

Born, R.T., and Bradley, D.C. (2005). Structure and function of visual area MT. Annu. Rev. Neurosci. *28*, 157–189.

Born, R.T., and Tootell, R.B. (1992). Segregation of global and local motion processing in primate middle temporal visual area. Nature *357*, 497–499.

Braddick, O. (1993). Segmentation versus integration in visual motion processing. Trends Neurosci. *16*, 263–268.

Bruce, C., Desimone, R., and Gross, C.G. (1981). Visual properties of neurons in a polysensory area in superior temporal sulcus of the macaque. J. Neurophysiol. *46*, 369–384.

Burkhalter, A., and Van Essen, D.C. (1986). Processing of color, form and disparity information in visual areas VP and V2 of ventral extrastriate cortex in the macaque monkey. J. Neurosci. *6*, 2327–2351.

Cavanaugh, J.R., Bair, W., and Movshon, J.A. (2002). Nature and interaction of signals from the receptive field center and surround in macaque V1 neurons. J. Neurophysiol. *88*, 2530–2546.

Chen, S.C., Morley, J.W., and Solomon, S.G. (2015). Spatial precision of population activity in primate area MT. J. Neurophysiol. *114*, 869–878.

Chen, M., Li, P., Zhu, S., Han, C., Xu, H., Fang, Y., Hu, J., Roe, A.W., and Lu, H.D. (2016). An Orientation Map for Motion Boundaries in Macaque V2. Cereb. Cortex *26*, 279–287.

Colby, C.L., Duhamel, J.R., and Goldberg, M.E. (1993). Ventral intraparietal area of the macaque: Anatomic location and visual response properties. J. Neurophysiol. *69*, 902–914.

Desimone, R., and Schein, S.J. (1987). Visual properties of neurons in area V4 of the macaque: Sensitivity to stimulus form. J. Neurophysiol. *57*, 835–868.

Desimone, R., and Ungerleider, L.G. (1986). Multiple visual areas in the caudal superior temporal sulcus of the macaque. J. Comp. Neurol. *248*, 164–189.

DeYoe, E.A., and Van Essen, D.C. (1985). Segregation of efferent connections and receptive field properties in visual area V2 of the macaque. Nature *317*, 58–61.

El-Shamayleh, Y., Kumbhani, R.D., Dhruv, N.T., and Movshon, J.A. (2013). Visual response properties of V1 neurons projecting to V2 in macaque. J. Neurosci. *33*, 16594–16605.

Fanini, A., and Assad, J.A. (2009). Direction selectivity of neurons in the macaque lateral intraparietal area. J. Neurophysiol. *101*, 289–305.

Felleman, D.J., and Kaas, J.H. (1984). Receptive-field properties of neurons in middle temporal visual area (MT) of owl monkeys. J. Neurophysiol. *52*, 488–513.

Felleman, D.J., and Van Essen, D.C. (1987). Receptive field properties of neurons in area V3 of macaque monkey extrastriate cortex. J. Neurophysiol. *57*, 889–920.

Felleman, D.J., and Van Essen, D.C. (1991). Distributed hierarchical processing in the primate cerebral cortex. Cereb. Cortex *1*, 1–47.

Ferrera, V.P., Nealey, T.A., and Maunsell, J.H. (1994). Responses in macaque visual area V4 following inactivation of the parvocellular and magnocellular LGN pathways. J. Neurosci. *14*, 2080–2088.

Foster, K.H., Gaska, J.P., Nagler, M., and Pollen, D.A. (1985). Spatial and temporal frequency selectivity of neurones in visual cortical areas V1 and V2 of the macaque monkey. J. Physiol. *365*, 331–363.

Galletti, C., Battaglini, P.P., and Fattori, P. (1991). Functional Properties of Neurons in the Anterior Bank of the Parieto-occipital Sulcus of the Macaque Monkey. Eur. J. Neurosci. *3*, 452–461.

Gegenfurtner, K.R., Kiper, D.C., and Fenstemaker, S.B. (1996). Processing of color, form, and motion in macaque area V2. Vis. Neurosci. *13*, 161–172.

Gegenfurtner, K.R., Kiper, D.C., and Levitt, J.B. (1997). Functional properties of neurons in macaque area V3. J. Neurophysiol. *77*, 1906–1923.

Gur, M., and Snodderly, D.M. (2007). Direction selectivity in V1 of alert monkeys: Evidence for parallel pathways for motion processing. J. Physiol. *585*, 383–400.

Gur, M., Kagan, I., and Snodderly, D.M. (2005). Orientation and direction selectivity of neurons in V1 of alert monkeys: Functional relationships and laminar distributions. Cereb. Cortex *15*, 1207–1221.

Hawken, M.J., Parker, A.J., and Lund, J.S. (1988). Laminar organization and contrast sensitivity of direction-selective cells in the striate cortex of the Old World monkey. J. Neurosci. *8*, 3541–3548.

Hildreth, E.C., and Koch, C. (1987). The analysis of visual motion: From computational theory to neuronal mechanisms. Annu. Rev. Neurosci. *10*, 477–533.

Huang, X., Albright, T.D., and Stoner, G.R. (2007). Adaptive surround modulation in cortical area MT. Neuron *53*, 761–770.

Hubel, D.H. (1959). Single unit activity in striate cortex of unrestrained cats. J. Physiol. *147*, 226–238.

Hubel, D.H., and Wiesel, T.N. (1968). Receptive fields and functional architecture of monkey striate cortex. J. Physiol. *195*, 215–243.

Jones, H.E., Grieve, K.L., Wang, W., and Sillito, A.M. (2001). Surround suppression in primate V1. J. Neurophysiol. *86*, 2011–2028.

Kohn, A., and Movshon, J.A. (2004). Adaptation changes the direction tuning of macaque MT neurons. Nat. Neurosci. *7*, 764–772.

Lamme, V.A. (1995). The neurophysiology of figure-ground segregation in primary visual cortex. J. Neurosci. *15*, 1605–1615.

Lamme, V.A., Zipser, K., and Spekreijse, H. (1998). Figure-ground activity in primary visual cortex is suppressed by anesthesia. Proc. Natl. Acad. Sci. USA *95*, 3263–3268.

Levitt, J.B., Kiper, D.C., and Movshon, J.A. (1994). Receptive fields and functional architecture of macaque V2. J. Neurophysiol. *71*, 2517–2542.

Li, P., Zhu, S., Chen, M., Han, C., Xu, H., Hu, J., Fang, Y., and Lu, H.D. (2013). A motion direction preference map in monkey V4. Neuron *78*, 376–388.

Lu, H.D., Chen, G., Tanigawa, H., and Roe, A.W. (2010). A motion direction map in macaque V2. Neuron *68*, 1002–1013.

Marcar, V.L., Xiao, D.K., Raiguel, S.E., Maes, H., and Orban, G.A. (1995). Processing of kinetically defined boundaries in the cortical motion area MT of the macaque monkey. J. Neurophysiol. *74*, 1258–1270.

Marcar, V.L., Raiguel, S.E., Xiao, D., and Orban, G.A. (2000). Processing of kinetically defined boundaries in areas V1 and V2 of the macaque monkey. J. Neurophysiol. *84*, 2786–2798.

Maunsell, J.H., and Van Essen, D.C. (1983). Functional properties of neurons in middle temporal visual area of the macaque monkey. I. Selectivity for stimulus direction, speed, and orientation. J. Neurophysiol. *49*, 1127–1147.

Mauss, A.S., Vlasits, A., Borst, A., and Feller, M. (2017). Visual circuits for direction selectivity. Annu. Rev. Neurosci. *40*, 211–230.

Mendoza-Halliday, D., Torres, S., and Martinez-Trujillo, J.C. (2014). Sharp emergence of feature-selective sustained activity along the dorsal visual pathway. Nat. Neurosci. *17*, 1255–1262.

Mikami, A., Newsome, W.T., and Wurtz, R.H. (1986). Motion selectivity in macaque visual cortex. I. Mechanisms of direction and speed selectivity in extrastriate area MT. J. Neurophysiol. *55*, 1308–1327.

Miura, K., Inaba, N., Aoki, Y., and Kawano, K. (2014). Difference in visual motion representation between cortical areas MT and MST during ocular following responses. J. Neurosci. *34*, 2160–2168.

Mountcastle, V.B., Motter, B.C., Steinmetz, M.A., and Sestokas, A.K. (1987). Common and differential effects of attentive fixation on the excitability of parietal and prestriate (V4) cortical visual neurons in the macaque monkey. J. Neurosci. *7*, 2239–2255.

Movshon, J.A., and Newsome, W.T. (1996). Visual response properties of striate cortical neurons projecting to area MT in macaque monkeys. J. Neurosci. *16*, 7733–7741.

Movshon, J.A., Gizzi, M.S., and Newsome, W.T. (1985). The analysis of visual moving patterns. In Pattern Recognition Mechanisms, C. Chagas, R. Gattass, and C. Gross, eds. (Springer), pp. 117–151.

Nassi, J.J., and Callaway, E.M. (2007). Specialized circuits from primary visual cortex to V2 and area MT. Neuron *55*, 799–808.

Nassi, J.J., Lyon, D.C., and Callaway, E.M. (2006). The parvocellular LGN provides a robust disynaptic input to the visual motion area MT. Neuron *50*, 319–327.

Nawrot, M., Shannon, E., and Rizzo, M. (1996). The relative efficacy of cues for two-dimensional shape perception. Vision Res. *36*, 1141–1152.

Nowak, L.G., Munk, M.H., Girard, P., and Bullier, J. (1995). Visual latencies in areas V1 and V2 of the macaque monkey. Vis. Neurosci. *12*, 371–384.

Orban, G.A. (1996). Physiology of motion and vision in primates. In Functional Neuroanatomy of Motion and Vision, G. Scotti and D. Le Bihan, eds. (Milan: Edizioni del Centauro-Udine), pp. 23–28.

Orban, G.A., Kennedy, H., and Bullier, J. (1986). Velocity sensitivity and direction selectivity of neurons in areas V1 and V2 of the monkey: Influence of eccentricity. J. Neurophysiol. *56*, 462–480.

Orban, G.A., Fize, D., Peuskens, H., Denys, K., Nelissen, K., Sunaert, S., Todd, J., and Vanduffel, W. (2003). Similarities and differences in motion processing between the human and macaque brain: Evidence from fMRI. Neuropsychologia *41*, 1757–1768.

Pack, C.C., Hunter, J.N., and Born, R.T. (2005). Contrast dependence of suppressive influences in cortical area MT of alert macaque. J. Neurophysiol. *93*, 1809–1815.

Palmer, L.A., and Nafziger, J.S. (2002). Effects of surround motion on receptive-field gain and structure in area 17 of the cat. Vis. Neurosci. *19*, 335–353.

Perge, J.A., Borghuis, B.G., Bours, R.J., Lankheet, M.J., and van Wezel, R.J. (2005). Dynamics of directional selectivity in MT receptive field centre and surround. Eur. J. Neurosci. *22*, 2049–2058.

Peterhans, E., and von der Heydt, R. (1993). Functional organization of area V2 in the alert macaque. Eur. J. Neurosci. *5*, 509–524.

Ponce, C.R., Lomber, S.G., and Born, R.T. (2008). Integrating motion and depth via parallel pathways. Nat. Neurosci. *11*, 216–223.

Ponce, C.R., Hunter, J.N., Pack, C.C., Lomber, S.G., and Born, R.T. (2011). Contributions of indirect pathways to visual response properties in macaque middle temporal area MT. J. Neurosci. *31*, 3894–3903.

Priebe, N.J., Cassanello, C.R., and Lisberger, S.G. (2003). The neural representation of speed in macaque area MT/V5. J. Neurosci. *23*, 5650–5661.

Priebe, N.J., Lisberger, S.G., and Movshon, J.A. (2006). Tuning for spatiotemporal frequency and speed in directionally selective neurons of macaque striate cortex. J. Neurosci. *26*, 2941–2950.

Qian, N., and Andersen, R.A. (1994). Transparent motion perception as detection of unbalanced motion signals. II. Physiology. J. Neurosci. *14*, 7367–7380.

Raiguel, S., Van Hulle, M.M., Xiao, D.K., Marcar, V.L., and Orban, G.A. (1995). Shape and spatial distribution of receptive fields and antagonistic motion surrounds in the middle temporal area (V5) of the macaque. Eur. J. Neurosci. *7*, 2064–2082.

Raiguel, S.E., Xiao, D.K., Marcar, V.L., and Orban, G.A. (1999). Response latency of macaque area MT/V5 neurons and its relationship to stimulus parameters. J. Neurophysiol. *82*, 1944–1956.

Regan, D. (1986). Form from motion parallax and form from luminance contrast: Vernier discrimination. Spat. Vis. *1*, 305–318.

Regan, D. (1989). Orientation discrimination for objects defined by relative motion and objects defined by luminance contrast. Vision Res. *29*, 1389–1400.

Regan, D., and Hamstra, S.J. (1992). Dissociation of orientation discrimination from form detection for motion-defined bars and luminance-defined bars: Effects of dot lifetime and presentation duration. Vision Res. *32*, 1655–1666.

Rosenberg, A., Wallisch, P., and Bradley, D.C. (2008). Responses to direction and transparent motion stimuli in area FST of the macaque. Vis. Neurosci. *25*, 187–195.

Sceniak, M.P., Hawken, M.J., and Shapley, R. (2001). Visual spatial characterization of macaque V1 neurons. J. Neurophysiol. *85*, 1873–1887.

Shipp, S., and Zeki, S. (2002). The functional organization of area V2, I: Specialization across stripes and layers. Vis. Neurosci. *19*, 187–210.

Siegel, R.M., and Read, H.L. (1997). Analysis of optic flow in the monkey parietal area 7a. Cereb. Cortex *7*, 327–346.

Sincich, L.C., and Horton, J.C. (2003). Independent projection streams from macaque striate cortex to the second visual area and middle temporal area. J. Neurosci. *23*, 5684–5692.

Sincich, L.C., and Horton, J.C. (2005). The circuitry of V1 and V2: Integration of color, form, and motion. Annu. Rev. Neurosci. *28*, 303–326.

Smith, M.A., Majaj, N.J., and Movshon, J.A. (2005). Dynamics of motion signaling by neurons in macaque area MT. Nat. Neurosci. *8*, 220–228.

Smolyanskaya, A., Haefner, R.M., Lomber, S.G., and Born, R.T. (2015). A modality-specific feedforward component of choice-related activity in MT. Neuron *87*, 208–219.

Snowden, R.J., Treue, S., Erickson, R.G., and Andersen, R.A. (1991). The response of area MT and V1 neurons to transparent motion. J. Neurosci. *11*, 2768–2785.

Tadin, D., and Lappin, J.S. (2005). Linking psychophysics and physiology of center-surround interactions in visual motion processing. In Seeing Spatial Form, L.R. Harris and M.R.M. Jenkin, eds. (Oxford University Press), pp. 279–314.

Tamura, H., Sato, H., Katsuyama, N., Hata, Y., and Tsumoto, T. (1996). Less segregated processing of visual information in V2 than in V1 of the monkey visual cortex. Eur. J. Neurosci. *8*, 300–309.

Tanaka, K., Hikosaka, K., Saito, H., Yukie, M., Fukada, Y., and Iwai, E. (1986). Analysis of local and wide-field movements in the superior temporal visual areas of the macaque monkey. J. Neurosci. *6*, 134–144.

Van Essen, D.C., and Zeki, S.M. (1978). The topographic organization of rhesus monkey prestriate cortex. J. Physiol. *277*, 193–226.

Vanduffel, W., Fize, D., Mandeville, J.B., Nelissen, K., Van Hecke, P., Rosen, B.R., Tootell, R.B., and Orban, G.A. (2001). Visual motion processing investigated using contrast agent-enhanced fMRI in awake behaving monkeys. Neuron *32*, 565–577.

von der Heydt, R., Peterhans, E., and Baumgartner, G. (1984). Illusory contours and cortical neuron responses. Science *224*, 1260–1262.

von der Heydt, R., Zhou, H., and Friedman, H.S. (2000). Representation of stereoscopic edges in monkey visual cortex. Vision Res. *40*, 1955–1967.

Xiao, D.K., Raiguel, S., Marcar, V., and Orban, G.A. (1997). The spatial distribution of the antagonistic surround of MT/V5 neurons. Cereb. Cortex *7*, 662–677.

Xu, H., Han, C., Chen, M., Li, P., Zhu, S., Fang, Y., Hu, J., Ma, H., and Lu, H.D. (2016). Rivalry-like neural activity in primary visual cortex in anesthetized monkeys. J. Neurosci. *36*, 3231–3242.

Zhang, B., Zheng, J., Watanabe, I., Maruko, I., Bi, H., Smith, E.L., 3rd, and Chino, Y. (2005). Delayed maturation of receptive field center/surround mechanisms in V2. Proc. Natl. Acad. Sci. USA *102*, 5862–5867.

Zirnsak, M., Steinmetz, N.A., Noudoost, B., Xu, K.Z., and Moore, T. (2014). Visual space is compressed in prefrontal cortex before eye movements. Nature *507*, 504–507.

STAR★METHODS

KEY RESOURCES TABLE

REAGENT or RESOURCE	SOURCE	IDENTIFIER
Experimental Models: Organisms/Strains		
Macaca mulatta	Beijing Institute of Xieerxin Bology Resource;	http://www.xexbio.com/
	Suzhou Xishan Zhongke animal Company, Ltd;	http://xsdw.bioon.com.cn/
Software and Algorithms		
MATLAB	MathWorks	MATLAB-R2012b

CONTACT FOR REAGENT AND RESOURCE SHARING

Further information and requests for resources and reagents should be directed to and will be fulfilled by the Lead Contact, Haidong D. Lu (haidong@bnu.edu.cn).

EXPERIMENTAL MODEL AND SUBJECT DETAILS

A total of 9 hemispheres from 8 adult male macaque monkeys (Macaca mulatta) were examined. All procedures were performed in accordance with the National Institutes of Health Guidelines and were approved by the Institutional Animal Care and Use Committee (Institute of Neuroscience, Chinese Academy of Sciences, and Beijing Normal University).

METHOD DETAILS

Intrinsic signal optical imaging

Chronic optical/recording chambers were implanted as described previously (Li et al., 2013; Xu et al., 2016). The only difference is that we used silicon artificial dura instead of tecoflax dura to allow electrode penetration (Arieli et al., 2002). Chamber locations were close to the midline. The eccentricity of the visual field corresponding to the exposed V1/V2 was 1-5°.

Before electrophysiological experiments, optical images were collected in the first 1-2 experiments, during which basic functional maps of V1 and V2 were obtained. Monkeys were artificially ventilated and anesthetized with thiopental sodium (induction 10 mg/kg, maintenance 3 mg/kg/hr intravenously [i.v.], for one monkey) or propofol (induction 5-10 mg/kg, maintenance 5-10 mg/kg/hr, i.v., for 7 monkeys). Anesthetic depth was assessed continuously via monitoring heart rate, end-tidal CO_2, and blood oximetry. Rectal temperature was maintained at ~38°C. Animals were paralyzed (vecuronium bromide, induction 0.25 mg/kg, maintenance 0.05-0.1 mg/kg/hr, i.v.) and respirated. Pupils were dilated (atropine sulfate 1%) and eyes were fitted with contact lenses of appropriate curvature to focus on a stimulus screen 57 cm from the eyes. The brain was stabilized with agar and imaged through a cover glass. Images of cortical reflectance changes (intrinsic hemodynamic signals) corresponding to local cortical activity were acquired (Imager 3001, Optical Imaging Inc., Germantown, NY) with 632 nm illumination. Image size was 540 × 654 pixels representing ~18 × 22 mm field of view. Each stimulus set was normally imaged 1-2 times. As reported in previous studies (e.g., Lu et al., 2010), direction maps are highly replicable from the same cortical region in V2, thus, we did not systematically test the biological replication of V2 direction maps in this study. Consistency of the imaging system (technical replication) was carefully monitored throughout the experiments and over different experimental sessions.

Functional maps were calculated based on t tests as previously described (Li et al., 2013). To calculate the domain size of direction domains, we first obtained 4 direction maps (0° versus 180°; 45° versus 225°; 90° versus 270°; 135° versus 315°) with t tests. Pixels with significant differences ($p < 0.05$, two tailed t test) were included in the analysis. The length and width of each domain were measured manually. We took the average of the length and width of each domain as their domain size.

The coverage of V2 direction domains was calculated by dividing the total direction domain size by its corresponding V2 size in CO cycle bases (i.e., to make sure a full cycle of thin-pale-thick-pale were included).

Map-guided single-cell recordings

After initial imaging experiments, electrophysiological single-cell extracellular recordings were performed as described previously (Li et al., 2013). For each chamber, recordings were carried out once a week and each recording session lasted for ~10 hours. The animal preparation and anesthesia were the same as those described in the imaging experiments. The cortex was stabilized by a coverslip with a hole in the targeted region. The locations of V2 direction domains were first marked on a surface blood vessel map (Figure 2E). Under a surgical microscope, a tungsten microelectrode (impedance 1–4 MΩ at 1 kHz, FHC) was lowered into the cortex (Nan system) targeting the center of a specific direction domain. Neural activity was amplified at 1 k or 10 k gain (Model 1800,

A-M Systems) and digitized at a sampling rate of 20-50 kHz (Power 1401, Cambridge Electronic Design Ltd.). Once a single cell was isolated, its CRF was plotted using a manually controlled bar and/or grating stimulus. Then, a battery of computer-controlled stimuli was presented in its RF for quantitative characterization (see Figure S1). Due to time limitation, for most neurons, most stimulus sets (described below) were tested once. For a subset of neurons, some of the stimuli were repeated during the recording session (biological replication), and the responses of the neurons to the repeated tests were always consistent. Cells without obvious visual responses (normally had a high spontaneous response level, but difficult to map their RF) were ignored. Single-cell activity was isolated and sorted online (Spike2, Cambridge Electronic Design Ltd.). During recording, the onset timing of each stimulus presentation was also recorded in a separate channel through a photo diode attached to a corner of the stimulus screen. Each stimulus was normally tested for 15-50 trials, trial-by-trial variations were reported whenever applicable (error bars). During the experiment, system noise level and technical stability (technical replication) were continuously monitored to ensure the consistency of the recording system.

Visual stimuli for optical imaging

Visual stimuli were created using ViSaGe (Cambridge Research Systems Ltd) and displayed on a calibrated 21-inch CRT monitor (SONY CPD-G520) running at 100 Hz refreshing rate. Only black/white stimuli were used in this study. The luminance for white stimuli was 145.6 cd/m^2 and black was 0.87 cd/m^2.

Stimulus for obtaining ocular dominance maps

Through a pair of mechanical shutters placed in front of the two eyes, monocular rectangle wave gratings (SF: 1.5 cycle/deg, TF: 8 Hz, duty cycle: 0.2, contrast: 100%, mean luminance: 14.6 cd/m^2) were presented at 4 different orientations for obtaining ocular dominance maps in V1. A total of 9 conditions were tested with at least 7 s ISI (black screen) between two successive conditions.

Stimulus for obtaining direction maps

Drifting RDs were used to obtain V2 direction maps (Lu et al., 2010). Direction maps in V2 can also be obtained with grating stimuli (Lu et al., 2010) but the map signal is often weaker. A patch of RDs (6 × 6° - 8 × 8°, density 6-10 dots/deg^2), within which 0.1° sized dots were drifting at 4-8 deg/s in one of 8 different directions. A total of 9 conditions were tested including a stationary condition. Each condition was presented for 4 s and separated by at least 7 s ISI (during which stationary RDs were presented).

MB stimuli

MB stimuli were similar to those used previously (Chen et al., 2016) except that the positions of the boundaries were not randomized among trials (Video S1). A square patch (8-12°) of RDs was divided into several horizontal or vertical strips (width 1°). RDs (dot size 0.1°, density 6-10 dots/deg^2, speed 4-8°/s) in neighboring strips were drifting at opposite directions (at 45° or 135° angle with respect to the strip borders). The motion boundaries were stationary during the 4 s stimulus presentation. A total of 17 stimulus conditions were tested, including 8 MB stimuli (see Video S1) (2 orientations: horizontal and vertical; 2 drifting axes: 45° and 135°; and 4 direction reversed versions), 8 temporal boundary (TB) stimuli (see Video S2) as controls, similar to those used in a previous study (Chen et al., 2016), in which dots in neighboring strips were drifting at the same directions (4 directions) but still created weak temporal boundaries at the borders of two neighboring strips, and a blank condition (stationary RDs). Each condition was presented for 4 s and separated by at least 7 s ISI (during which stationary RDs were presented).

Visual stimuli for single-cell recording

Visual stimuli were created and presented using the same setup as in the imaging experiments. Each stimulus presentation is normally 0.5 s, followed by 0.5 s inter-stimulus interval (ISI). For some cells, we also tested a longer duration (0.7-1 s). All stimuli were in black (0.87 cd/m^2) and white (145.6 cd/m^2), and were presented monocularly (normally the contralateral eye).

Direction test

To measure the direction selectivity of a neuron, a circular patch of sine-wave gratings or RDs, with the size adjusted to the RF of each neuron, was presented. For gratings, their orientations were perpendicular to their drifting directions, and the SF (1-2 cycle/deg) and TF (4-8 Hz) were optimized based on earlier manual tests. For RDs, each dot was 0.1°. The dots covered ~5% of the patch surface and moved coherently within the patch at a speed of 4-8° /sec. A total of 8 or 12 equally spaced moving directions were tested. Each condition lasted 0.5-1 s and was separated by a 0.5-1 s ISI during which a gray screen (for gratings) or a stationary RD patch (for RDs) was presented.

Two-dimensional position test

To determine the precise RF center location, we adopted the P2D test described by Xiao et al. (1997). The RF region (4 × 4°) were divided into a 5 × 5 grid, with each sub-region sized 0.8°. During the test, a small 0.8° circular patch of gratings (occasionally RDs), drifting in the cell's preferred direction, was presented randomly at one of these 25 possible locations. Each stimulus was presented for 0.3 s, separated by a 0.3 s black screen. The strongest response location was marked as the RF center, which was used for the subsequent tests.

Area summation test

In order to compare responses between DS and non-DS neurons, we used gratings in this test instead of RD (since gratings can effectively trigger both DS neurons and non-DS neurons). To measure the RF size and surround properties, circular square-wave gratings of different sizes (0.2, 0.4, 0.6, 0.8, 1, 2, 3, 4, 5, 6, 7°) were tested. The grating patch was centered at the RF center and drifted

in the neuron's preferred direction. Each stimulus was presented for 0.5-1 s. An equal luminance gray screen was presented during ISI for 0.5-1 s. RF size was calculated (see data analysis) and used in the subsequent tests.

Surround direction test

We tested how surround motion modulates the responses to preferred center stimulation. An 8° circular RD patch was divided into a center (circular patch) and a surround (an annulus) (Figure 4D). The size of the center patch was equal to the optimal stimulus size (RF size) obtained in the summation test. For all the stimulus conditions, center RDs always drifted in the neuron's preferred direction. Surround RDs drifted in 8 different directions (0, 45, 90, 135, 180, 225, 270, 315°) relative to the center direction. A total of 8 stimulus conditions were presented randomly. For some neurons (n = 31), we added a stationary surround condition. Each stimulus was presented for 0.5-1 s with a 0.5-1 s stationary RD ISI. RD stimuli were used here to avoid orientation contribution in grating tests and also to be comparable with the MB test described below.

Surround Asymmetry Test

We measured the spatial distributions of V2 DS neurons' surround. The stimuli were similar to those described by Xiao et al. (1997). A circular stimulus patch centered on the RF center, while a second circular patch was presented in one of eight positions surrounding the center patch at 45° intervals (Figure S6A). The diameter of the central patch was set to the neuron's optimal diameter. The peripheral patch (diameter = ~5°) touched the center patch, leaving no gap between the two patches. A control condition was included, in which only the center patch was presented in which stimulus moved in the neuron's preferred direction.

MB position test

To test neurons' responses to different MB positions, we presented the MB stimulus at different locations in relative to the neuron's RF. An illustration of the stimulus is shown in Video S3. A 10° square RD patch was divided into two parts (see Figure 5A). One part contained RDs drifted in the neuron's preferred direction, while dots in the other part drifted in the opposite direction. It created a virtual boundary at the border between these two RD patches. This virtual boundary was either horizontal or vertical. For each orientation, the boundary was presented at 7 different locations relative to the RF center, at a 0.5° step. For each of the horizontal and vertical boundary conditions, there were 14 boundary stimulus conditions. In half of the conditions, the directions of the dots in the two parts were switched. In the additional 2 conditions, the drifting directions of all the dots were the same, either in the neurons preferred direction or anti-preferred direction. This made up a total of 16 conditions for either horizontal or vertical tests. Each condition was presented for 0.5 s, with a 0.5-1 s stationary RD background as ISI. Total 43 neurons were tested with both horizontal and vertical stimuli.

Transparent motion test

We tested neurons' responses to transparent RD motion similar to those described by Snowden (Snowden et al., 1991). Two sets of RDs (density 12-20 dots/deg^2) drifted within a circular patch (size1-2°). One set of RDs always drifted at the neurons' preferred direction and speed (4-8 deg/s), while the other set drifted at one of 8 equally spaced directions at the same speed. The angles between the 8 test directions and the preferred direction were 0, 45, 90, 135, 180, 225, 270, and 315°. When the angle was 0°, only one set of RDs was presented (i.e., in this condition, the dot density is half of that in the other 7 conditions).

Plaid test

To test whether DS neurons were sensitive to pattern motion, we used plaid stimuli similar to those used in previous studies (Smith et al., 2005). Two sine-wave gratings (size 1-2°) were overlaid to form a plaid. The parameters of these two gratings were the same as those used in the direction test for a neuron, normally optimal for the neuron if these values were known, or SF = 1-2 cycle/deg, and TF = 4-8Hz when these values were not tested. Two gratings had a fixed orientation difference of 60°. The plaid drifted at 12 equally spaced directions and the drifting direction was always along the midline of the two grating orientations (i.e., offset in their orientations by 30°).

Spatiotemporal and speed tuning tests

To test the neuron's SF and TF tuning, a circular patch of sine-wave gratings was presented in the neuron's RF and drifted in the neurons' preferred direction. A full combination of five SFs (0.25, 0.5, 1, 2, 4 cycle/deg) and eight TFs (0.25, 0.5, 1, 2, 4, 8, 16, 32Hz) were tested, which made a total of 40 stimulus conditions. To test the neuron's speed tuning, a circular patch of RDs with different speeds (0.5, 1, 2, 4, 8, 16, 32 deg/s) were presented in the neuron's RF at its preferred direction. Each stimulus was presented for 0.5-1sec, with a gray screen (Spatiotemporal test) or stationary RD (RD speed tuning test) ISI for 0.5-1 s. Since these tests were performed before the area summation test, the stimulus size (1-2°) was determined based on the initial manual test to cover the classical RF.

Electrophysiological data analysis

Single cell data were first analyzed online with Spike2 software. When a neuron was identified, a spike shape template was created and subsequent online analysis was based on this template. In offline analysis, all recordings were sorted again. Neuronal responses to each condition were calculated by averaging the spike numbers during the stimulus presentation and subtracting the baseline activity 200 ms before stimulus onset. The neuronal responses were passed to a least-square nonlinear regression function ("nlinfit" in MATLAB, Mathworks) that fit the data by using the following equations or methods.

Analysis of direction tuning

Direction tuning curves were fitted with a von Mises function (Kohn and Movshon, 2004)

$$R = ae^{b\cos(\theta - xc)} + m$$

where θ is the stimulus direction, a is the amplitude of the tuning curve, *b* is the half-height width of the tuning curve, *xc* is the preferred direction, and m is this baseline level. For the 143 DS neurons recorded, all the goodness values (R^2) were > 0.7. The tuning bandwidth was measured from the fitted curve (See Figure S1D).

The direction index was calculated with the following equation (Albright, 1984; Movshon and Newsome, 1996):

$$DI = 1 - \frac{antipreferred\ response}{preferred\ response}$$

where the preferred response is the response to the preferred direction, and the antipreferred response is the response to the opposite direction of the preferred direction. Note that the baseline activity was subtracted from the responses, so the DI could be greater than 1 when the response to the opposite motion is weaker than baseline activity.

Locating the RF center

To get the RF center location in the P2D test, we first normalized the responses to each grid position (same as Zirnsak et al., 2014):

$$r_n' = \frac{r_n - \min r_n}{\max r_n - \min r_n}$$

where r_n' is the response after normalization, r_n is the original response value, and minr_n and maxr_n are the minimum and maximum response values in the 25 grids (before normalization), respectively. A finer map with pixel size of 0.05 was obtained by linear interpolation of the 25 normalized data. The strongest response region was defined as the RF center (see Figure S1J).

Analysis of RF size

In the area summation test, we fitted the response curves with a ratio of Gaussian function (RoG) as Cavanaugh described (Cavanaugh et al., 2002, see Figure 3B).

$$R(x) = \frac{k_c L_c(x)}{1 + k_s L_s(x)}$$

$$L_c(x) = \left(\frac{2}{\sqrt{\pi}} \int_0^x e^{-(y/wc)^2} dy \right)^2$$

$$L_s(x) = \left(\frac{2}{\sqrt{\pi}} \int_0^x e^{-(y/ws)^2} dy \right)^2$$

where X is the stimulus diameter, *Kc* and *Ks* are gains for the RF center and surround, L_c and L_s are the total squared responses of the center and surround, and *wc* and *ws* are the size of the center and surround (*wc* < *ws*). The optimal stimulus size was determined as the diameter corresponding to the peak response in the fitted function. Note that the responses to the blank stimulus (0 degree) were the neurons' baseline activities. As we subtracted the baseline responses from the original data before fitting the tuning curves, the baseline levels were 0 spikes/sec. All the goodness values (R^2) were > 0.7.

Analysis of surround features

To compare with the SI values of MT (Pack et al., 2005), the suppression index (SI) was calculated as follows:

$$SI = 100 \times (1 - R7/R\ \max)$$

where R7 is neuron's response when the stimulus size is 7° (the largest stimulus size in the test), and Rmax is the neuron's measured maximum response in the test. Larger SI means larger surround suppression.

To compare with V1 neurons' SI values. We adopted the methods described by Sceniak et al. (2001) with the following equations.

$$\mathrm{R(s)} = \mathrm{R_0} + K_e \int_{-s/2}^{s/2} e^{-(2y/a)^2} dy - K_i \int_{-s/2}^{s/2} e^{-(2y/b)^2} dy$$

$$SI = K_i b / K_e a$$

Where $\mathbf{R}_0$ is the spontaneous rate, s is the stimulus diameter, K_e and K_i are the gains for the RF center and surround, *a* and *b* are the estimated sizes of the center and surround.

In the surround direction test, we obtained 8 response values from 8 surround directions. The angle differences between the center (fixed) and the surround (variable) were (−135, −90, −45, 0, 45, 90, 135, 180°, see Figure 4D). By comparing the responses between 0 and 180° conditions, we separated neurons into two groups: neurons with strong modulation (MI > 0.5, see Figure 4F) and neurons with weak modulation (MI < 0.5).

To quantify the asymmetry of the surround, we calculated the unimodel selective index (USI) value as previously (Xiao et al., 1997) described.

$$USI = \frac{\sqrt{\left[\sum_{i=1}^{n} Si \cdot \sin(\alpha i)\right]^2 + \left[\sum_{i=1}^{n} Si \cdot \cos(\alpha i)\right]^2}}{\sum_{i=1}^{n} Si}$$

where n = 8 (the number of surround positions tested), Si is the surround inhibition elicited by the stimulus located at position i, and αi is the angle between the direction of the stimulus motion and the line connecting the RF center to the center of the surround stimulus.

Analysis of pattern integration

For plaid response data, as the standard methods (Movshon et al., 1985), we calculated partial correlations (R_p and R_c below) and then converted them to Z-scores (Z_p and Z_c) based on the following equations:

$$R_p = \frac{(r_p - r_c r_{pc})}{\sqrt{(1 - r_c^2)(1 - r_{pc}^2)}} \quad R_c = \frac{(r_c - r_p r_{pc})}{\sqrt{(1 - r_p^2)(1 - r_{pc}^2)}}$$

$$Z_p = \frac{0.5 \ln\left(\frac{1 + R_p}{1 - R_p}\right)}{\sqrt{1/df}} \quad Z_c = \frac{0.5 \ln\left(\frac{1 + R_c}{1 - R_c}\right)}{\sqrt{1/df}}$$

where r_p and r_c are the correlations of the actual responses with pattern and component predictions respectively. r_{pc} is the correlation of the two predictions; df is the degree of freedom, as there were 12 directions in the tuning curve, $df = 9$. We used Z_p-$Z_c = \pm 1.28$ as a criterion for separating neurons into different groups in the correlation graph (see Figure S4B).

Analysis of speed selectivity

In the spatiotemporal response tuning test (Priebe et al., 2003), we tested 40 combinations of SF (5 conditions) and TF (8 conditions). The results were presented in Figure S3. We first identified a neuron's preferred SF and TF based on the response amplitudes. To investigate the SF-TF tuning dependency, we fitted the SF tuning curve and the TF tuning curve separately with Gaussian functions (RD speed tuning curves were also fitted with the Gaussian function, see Figure S1E; All the goodness values (R^2) were > 0.7). These fitting curves were then used to calculate two models: the SF-TF-independent model and speed-tuned model. The SF-TF-independent model was obtained by calculating the outer product of the SF and TF tuning curves. For the speed-tuned model, the TF tuning curve was shifted as a function of SF so that the preferred speed was independent of the SF. Partial correlations of the measured response with two models were obtained using the following equations:

$$R_{indep} = \frac{r_i - r_s \times r_{is}}{\sqrt{(1 - r_s^2)(1 - r_{is}^2)}} \quad R_{speed} = \frac{r_s - r_i \times r_{is}}{\sqrt{(1 - r_i^2)(1 - r_{is}^2)}}$$

where R_{indep} and R_{speed} are two partial correlations, r_i and r_s are correlations of the measured response with independent model and speed mode, respectively. r_{is} is the correlation of the two models. The separation lines were p = 0.05 in Figure S3E.

Analysis of time latency

The response delay calculation was similar to that described in Huang's work (Huang et al., 2007). Data from the spatiotemporal tuning test were used. We first obtained post-stimulus time histograms (PSTHs) with a bin size of 10 ms. This PSTHs were smoothed with a Savitzky-Golay filter. The mean and standard deviation of spontaneous activity were obtained from the 200 ms pre-stimulus period. From the stimulus onset, if a neuron's response exceeded its spontaneous level by 1, 1.5 and 2 standard deviations in 3 consecutive bins (see Figure S1F), the first bin time was recorded as the neuron's response delay.

QUANTIFICATION AND STATISTICAL ANALYSIS

Data were presented as mean ± Standard Deviation (SD) unless otherwise indicated. Two-tailed Student's t test was used to find the pixels that show significant response difference between two different visual stimuli. At least 30 repeats were conducted for each visual stimuli during the imaging. Wilcoxon test and Kolmogorov-Smimov test were used to compare the responses between DS neurons and non-DS neurons, or the neurons' responses between different visual stimuli. Each group contains at least 40 neurons. Spearman test was used to estimate the correlation between two variables. $p < 0.05$ was considered to be statistically significant.

Cell Reports, Volume *25*

Supplemental Information

Visual Motion Processing in Macaque V2

Jiaming Hu, Heng Ma, Shude Zhu, Peichao Li, Haoran Xu, Yang Fang, Ming Chen, Chao Han, Chen Fang, Xingya Cai, Kun Yan, and Haidong D. Lu

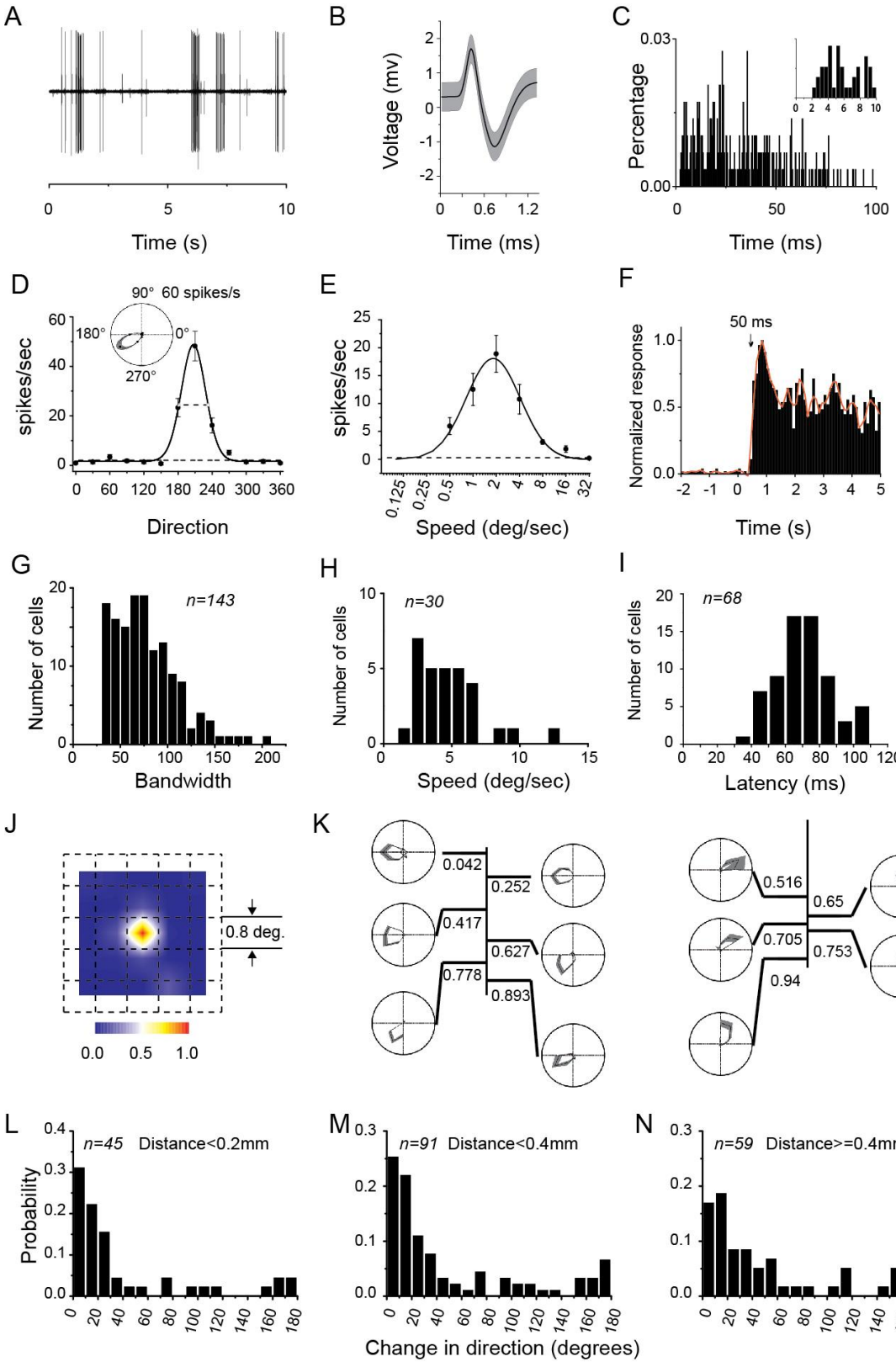
A
Time (s)
B
Voltage (mv)
Time (ms)
C
Percentage
Time (ms)
D
90° 60 spikes/s
180°
0°
270°
spikes/sec
Direction
E
spikes/sec
Speed (deg/sec)
F
50 ms
Normalized response
Time (s)
G
n=143
Number of cells
Bandwidth
H
n=30
Number of cells
Speed (deg/sec)
I
n=68
Number of cells
Latency (ms)
J
0.8 deg.
0.0 0.5 1.0
K
0.042
0.252
0.417
0.627
0.778
0.893
0.516
0.65
0.705
0.753
0.94
L
n=45 Distance<0.2mm
Probability
M
n=91 Distance<0.4mm
Change in direction (degrees)
N
n=59 Distance>=0.4mm

Figure S1. Basic single-cell response properties. Related to Figure 2.

(A) Example of single-cell response spikes. (B) Waveform of a single-cell spike. Gray areas represent ± 1 SD. (C) Distribution of inter-spike intervals of a single neuron after spike sorting (n=815 Spikes). Insert shows a magnified version of the data between 0-10 ms, and all intervals were larger than 2 ms. Only neurons with inter-spike-intervals larger than 1.5 ms were included in the subsequent analysis. (D) An example neuron's direction tuning curve and corresponding polar plot. Dotted lines represent the half-height width (middle) and the baseline level (bottom), respectively. Error bars: ± SEM. (E) An example neuron's speed tuning curve obtained with a drifting RD. Error bars: ± SEM. (F) An example neuron's post-stimulus time histogram (PSTH) in SF/TF test. This example neuron has a response latency of 50 ms, see Methods for details. (G) Distribution of direction tuning bandwidths for V2 DS neurons. (H) Distribution of preferred speeds of the tested V2 DS neurons. (I) Distribution of response latencies of the tested V2 DS neurons. (J) The RF map of a V2 DS neuron obtained with two-dimensional position test (P2D test). The stimulus was a small patch of optimal gratings (size 0.8°) randomly displayed at 25 possible locations (5×5 grids). The classic RF size of this V2 DS neuron is approximately 1°. (K) Direction polar plots (normalized to maximum response) of neurons recorded in two example penetrations. Although small shifts of preferred directions were observed, most neurons recorded in the same penetration preferred the similar directions. Numbers represent the depths of the electrode tip measured from the reference position (0 mm, the depth at which the first neuronal response was encountered in a penetration). (L-N): Distributions of angular shifts of preferred directions for pairs of neurons in the same penetration with distance <0.2 mm (L), <0.4 mm (M), and >0.4 mm (N). Although the shifts increase over distance, they are mostly within 45 degrees, indicating a columnar organization for preferred directions - same as the results reported in MT (Albright , 1984).

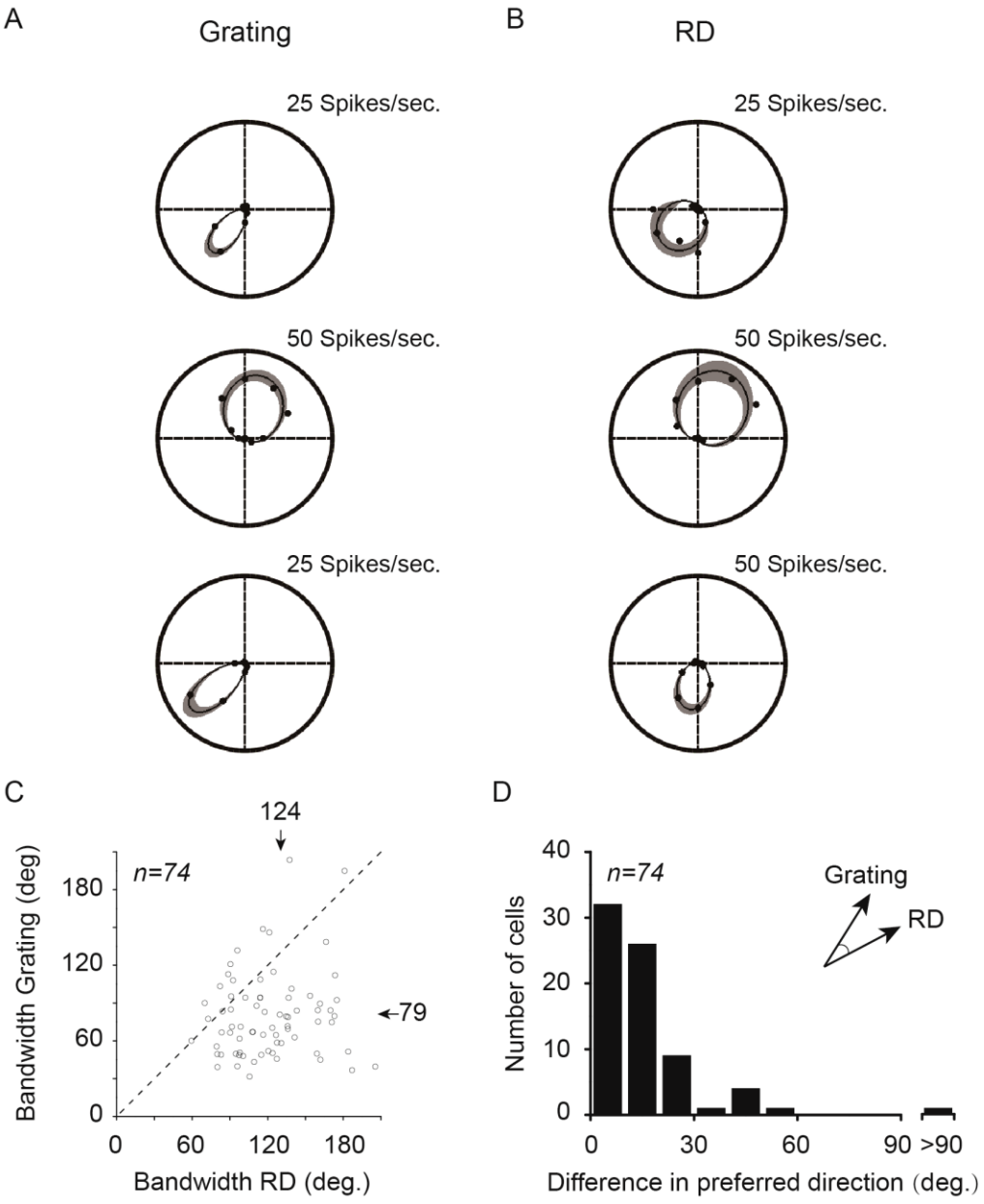

Figure S2. Similar directional selectivity to grating and RD stimuli. Related to Figure 2.

(A) Direction polar plots of 3 example neurons measured with drifting gratings. (B) Direction polar plots of the same 3 neurons measured with drifting RD stimuli. (C) Direction tuning curves measured with RD had wider bandwidth than those measured with gratings ($p<0.001$, Wilcoxon test). (D) Neurons exhibit similar direction preference for RD and grating stimuli. The difference between the optimal directions measured with RD and grating stimuli are mostly within 30 degrees. Data are represented as mean ± SEM.

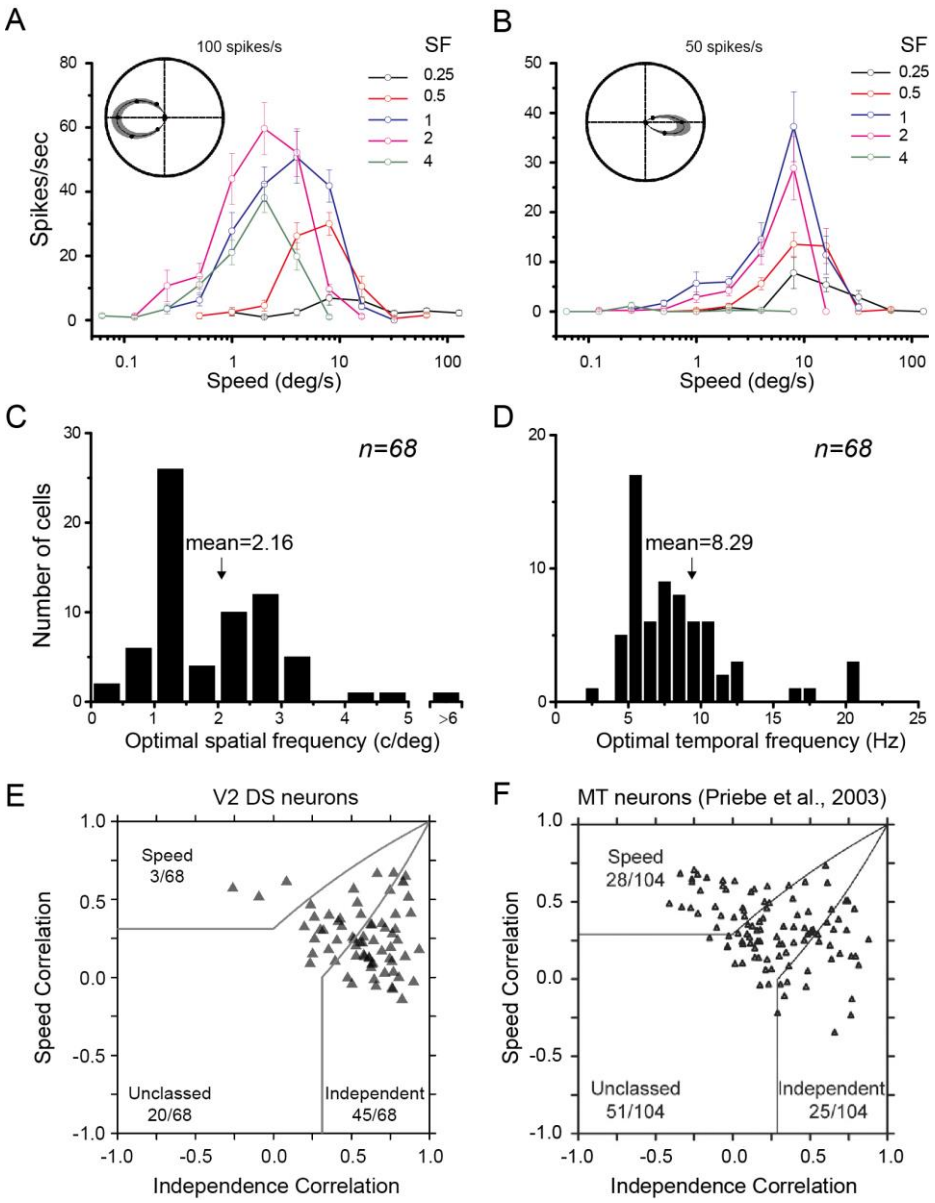

Figure S3. Majority V2 DS neurons are not speed tuned. Related to Results.

(A and B) Speed tuning curves of 2 example V2 DS neurons tested with gratings at different spatial frequencies. Inserts show the neurons' direction polar plots. Most tested neurons are like the example neuron 1 (A), whose preferred speed changed with the spatial frequencies of the grating stimuli. Only a few neurons show spatial frequency-independent speed tuning, like the example neuron 2 (B). Error bars: ± SEM. (C) Distribution of optimal SF, average SF=2.16 ± 2.81 cycle/deg (mean ± SD). (D) Distribution of optimal TF, average TF=8.29 ± 3.86 Hz (mean ± SD) for the same population of neurons shown in (C). (E) Scatter plot of speed correlation versus independence correlation. 68 V2 DS neurons were tested (from 6 monkeys), 3 neurons were classified as speed-tuned, 45 neurons were classified as spatiotemporal-independent, and 20 neurons were classified as unclassed. The gray lines indicate the dividing lines used to characterize the neuron types (p=0.05). (F) Scatter plot of speed correlation versus independence correlation for 104 neurons recorded in MT (reprinted from Figure 5D in Priebe et al. 2003, with permission). More neurons are speed-selective in area MT.

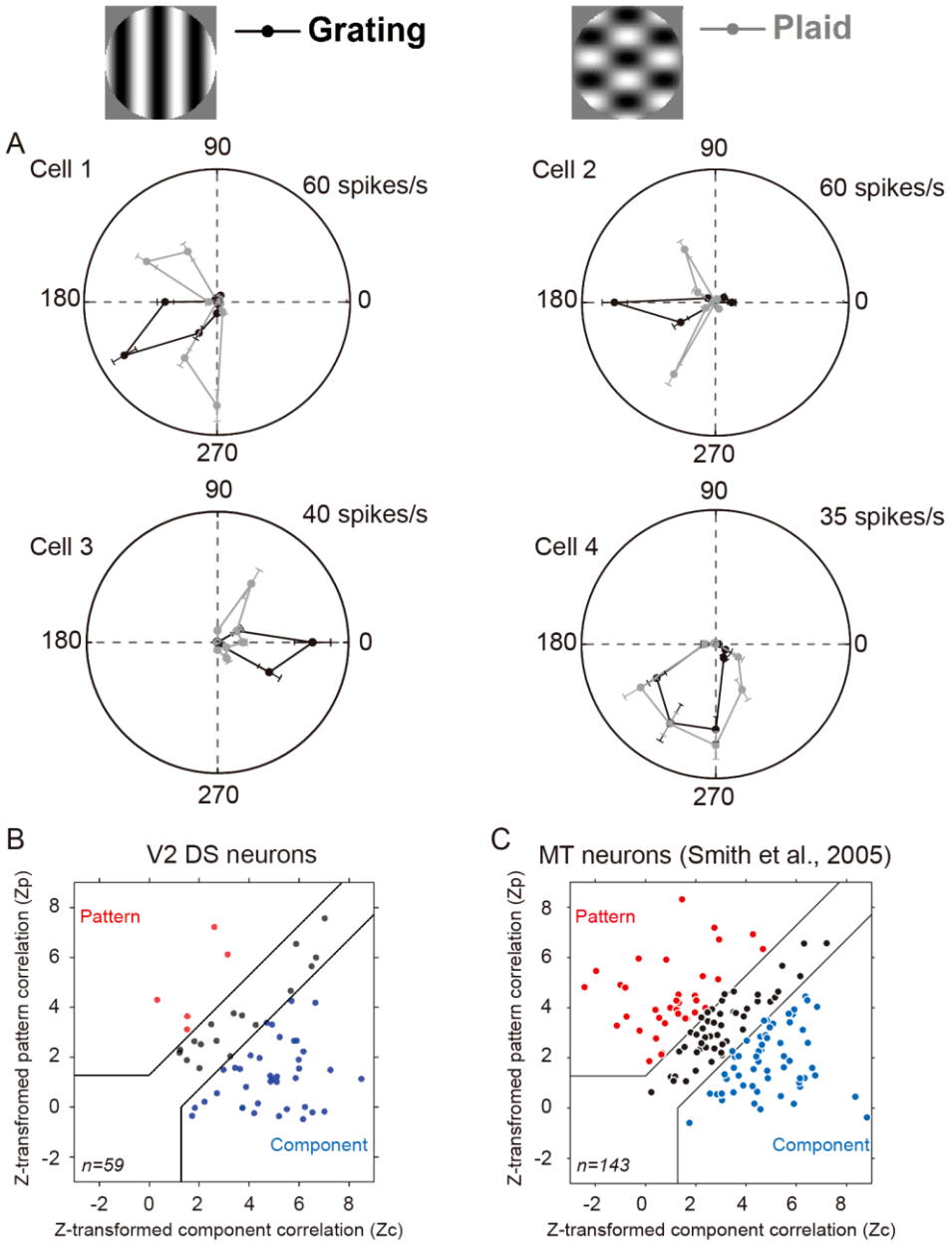

Figure S4. Majority V2 DS neurons are not pattern motion selective. Related to Results.

(A) Responses of 4 example V2 DS neurons to drifting gratings (black curves) and plaids (gray curves). Example neurons 1 and 2 exhibited 2 peaks in responding to plaids and the results can be predicted from their responses to grating components in the plaids. The example neuron 3 only showed one peak to one component grating; the other peak was not obvious. The example neuron 4 showed a direction preference for the plaid motion, not for the grating components in the plaid. Error bars: SEM. (B) Scatter plot of Z-transferred Rc and Rp for the 59 V2 DS neurons (from 6 monkeys) tested with plaid motion; only 5 neurons are classified as pattern-selective neurons (red dots). The solid gray lines (Same as Smith et al., 2005) indicate the class boundaries used to characterize the neuron type. (C) MT neurons' results for comparison (reprinted from Figure 3B in Smith et al., 2005, with permission). More neurons are pattern-selective in area MT than in V2. Data are represented as mean ± SEM.

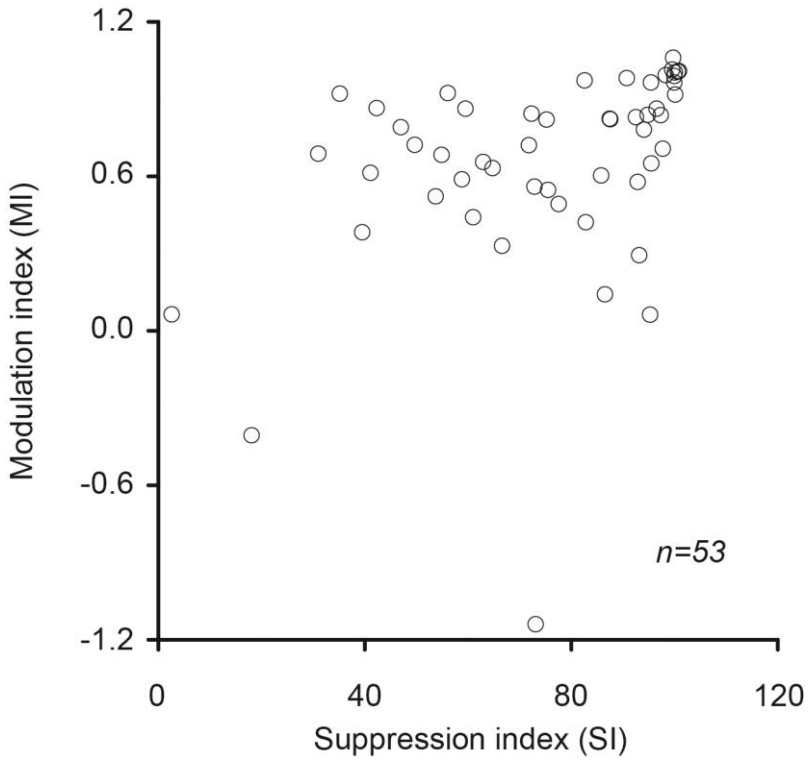

Figure S5. Correlation of MI and SI. Related to Figure 4.

Neurons have strong surround suppression (SI, as measured in summation test, see Figure 3C) also exhibit stronger modulation by surround direction (MI, as measured in center-surround test in Figure 4F, r=0.47, p=0.0004, Spearman test).

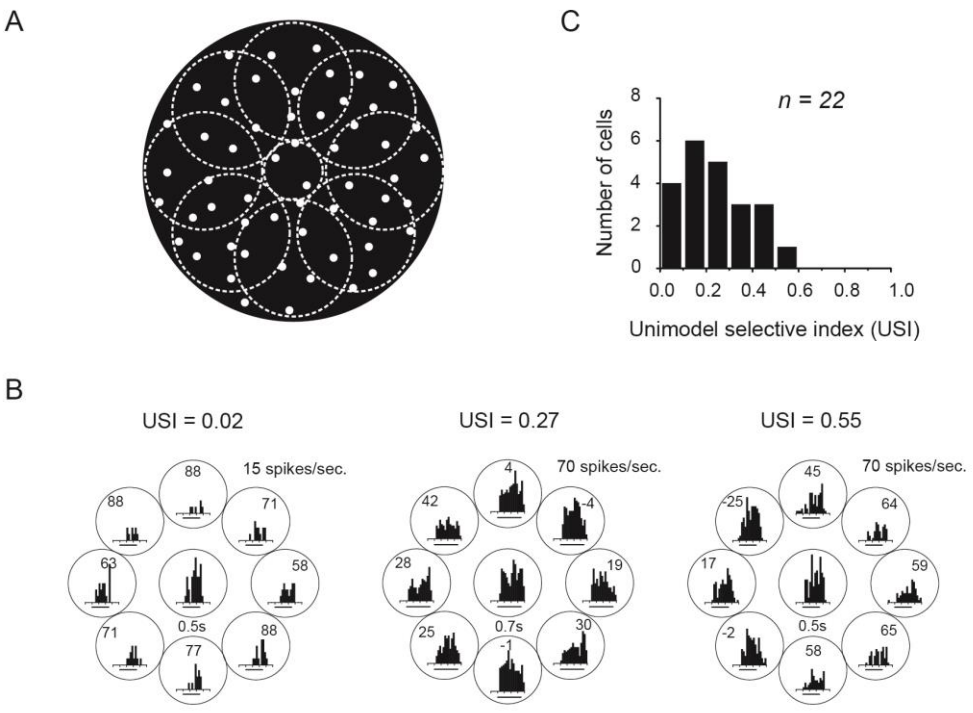

Figure S6. The spatial distribution of V2 DS neurons' surround. Related to Figure 4.

(A) Illustration of visual stimuli for mapping the surround structure. (B) Post-stimulus time histograms (PSTHs) of 3 example neurons. Responses to center-alone condition were presented in the center. Peripheral PSTHs at different locations show the responses in 8 corresponding center-surround conditions (values in the circles indicate suppressive index, 0 means no suppression, 100 means full suppression). Unimodel selective index (USI) values of these example cells are labeled on the top. (C) The distribution of USI, larger USI means stronger asymmetry.

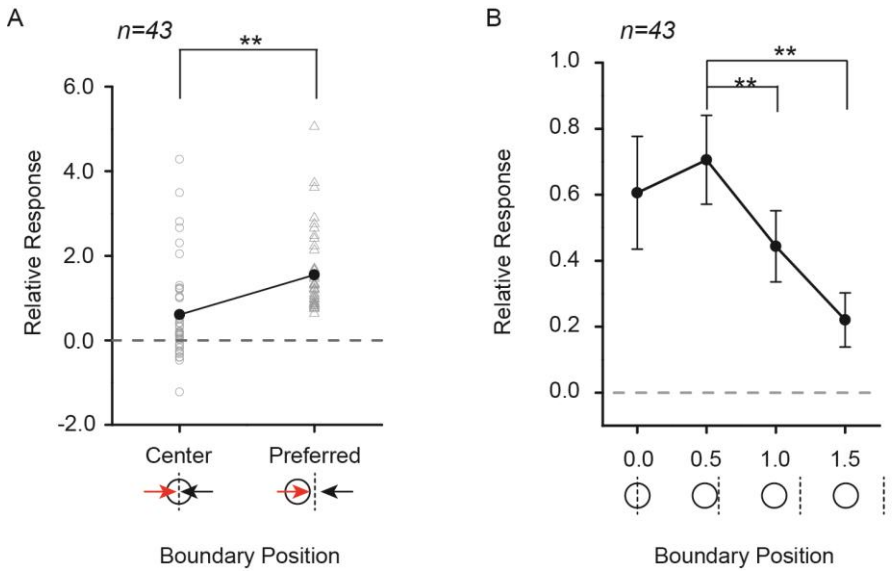

Figure S7. Population results for responses to MB position. Related to Figure 5.

(A) Response comparison of V2 DS neurons between two motion boundary conditions in MB position test (illustrated in Figure 5). Relative response (R) was calculated as: R=ln (Rtest/Rcoherence) where Rtest represents the response to the boundaries in different positions, Rcoherence is the response to coherent motions (average of the responses recorded in optimal and anti-optimal directions). Responses to the "Preferred" condition (boundary locates near the CRF border) were significantly stronger than the responses recorded in the "Center" condition (boundary locates in the CRF center, $p<0.01$, Wilcoxon test). (B) Similar to A, comparisons among the responses recorded in 4 MB positions. Results from the conditions that have the same distance between boundary and RF center were averaged (4 stimulus conditions, 2 different locations combined with 2 different orientations). After such average, the "0.5" condition still show stronger responses than "1.0" and "1.5" conditions ($p<0.01$, Wilcoxon test). Error bars: $\pm$ SEM.

Table S1. Percentages of DS neurons in different visual areas. Related to Figure 1.

Cortical Areas	Papers	CRS	Species	DS Neuron percentage	Mean Percentage
V1	Orban et al. (1986) Hawken et al. (1988) Tamura etal. (1996) Gur et al. (2005)	DI=1-n/p >=0.5 p/n >=3 DI=1-n/p >=0.7 DI=1-n/p >=0.5	7 7 4 6*	27% 17% (25/147) 16% (24/147) 20% (65/323)	20%
V2	Baizer et al. (1977) Van Essen and Zeki (1978) DeYoe and Van Essen (1985) Peterhans and von der Heydt (1993) Levitt et al. (1994) Gegenfurtner et al. (1996) Tamura et al. (1996)	-- -- DI=1-n/p >=0.7 DI=1-n/p >=0.5 DI=1-n/p >=0.67 DI=1-n/p >=0.7 DI=1-n/p >=0.7	3* 10 3 2* 13 8 4	12% (29/238) 8% (5/62) 7.2% (30/415) 28.9% (55/190) 15% (23/149) 19% (19/100) 32.3% (39/121)	17.5%
V3	Van Essen and Zeki (1978) Baizer (1982) Burkhalter and Van Essen (1986) Felleman and Van Essen (1987) Gegenfurtner et al. (1997)	-- -- DI=1-n/p >=0.7 DI=1-n/p >=0.7 DI=1-n/p >=0.7	10 5* N.A. 5 12	12% (5/40) 15% (11/75) 40% 40% (58/147) 39.7% (56/141)	29.3%
V4	Van Essen and Zeki (1978) Desimone and Schein (1987) Mountcastle et al. (1987) Ferrera et al. (1994)	-- DI=n/p <=0.3 DI=n/p <=0.5 DI=n/p<=0.5	10 7 4* 5	3% (2/74) 13% 18.9% (7/37) 24%	14.7%
MT	Maunsell and Van Essen (1983) Albright (1984) Mikami et al. (1986) Tanaka et al. (1986)	DI=p/n >=2 -- DI=1-n/p >=0.8 DI=n/p <0.1	5 8 5* 4	88% 84% 80% 76% (350/463)	82%
V3a	Galletti et al., 1991	--	2*	--	30%
V3v (VP)	Burkhalter and Van Essen (1986)	--	N.A.	--	13%
V4t	Desimone and Ungerleider (1986)	--	3	--	25%
MST	Tanaka et al. (1986) Mendoza-Halliday et al. (2014)	--	4 2*	54.9% 88%	54.9~88%
PO (V6)	Galletti et al. (1991)	--	2*	--	67%
LIP	Fanini and Assad (2009)	--	2*	--	61%
VIP	Colby et al. (1993)	--	3*	--	80%
7a	Siegel and Read (1997)	--	2*	--	60%
TEO (VOT, PIT**)**	Desimone and Ungerleider (1986)	--	3	--	~4%
FST	Rosenberg et al. (2008) Desimone and Ungerleider (1986)	--	3* 3	9.7% 32%	9.7 ~ 32%
STP	Bruce et al. (1981) Orban (1996, STPa)	--	5 N.A.	13% ~40%	13% (STP) 13~40% (STPa)

DS: Direction selective; CRS: criterion for response selectivity; n: response to nonpreferred direction; p: response to preferred direction; DI: direction index; N.A.: not available

*: Awake;

Table S2. RF property comparison for DS neurons in V1, V2 and MT. Related to Discussion.

	V1 DS	V2 DS	MT
Percentage of DS neurons	20%	17.5%	82%
RF size (deg)	0.95 (mean, **Layer 4B**, Jones et al., 2001) M.m. 1.8 (mean, **complex DS**, Bair and Movshon, 2004) M.m.	1.17 (mean)	~5 (**eccentricity =0~5**, Raiguel et al., 1995) M.m. 8 (mean, Bair and Movshon, 2004) M.m. 10.7 (mean, Perge et al., 2005) M.m.* Tenfold greater than v1 (Born and Bradley., 2005)
Surround type	Antagonistic (Lamme, 1995; Jones et al., 2001) M.m.* + M.m.	Antagonistic	Antagonistic and reinforcing (Born and Tootell., 1992) O.m.
Asymmetric surround	44% (**V1**, Jones et al., 2001) M.m.	11 / 22	**50 %** (**eccentricity =0~5**, Xiao et al., 1997) M.m.
Degree of suppression	67 (mean, **Layer 4B**, Jones et al., 2001) M.m.	71.4 (mean) 74.2 (median)	63 (median, Raiguel et al., 1995) M.m. 35 (median, Pack et al., 2005) M.m.*
Pattern selectivity	1/38 (**V1**, Movshon and Newsome, 1996) M.m.	5/59	36/143 (Smith et al., 2005) M.m.
Response to transparent motion (RF center)	Weak modulation (**V1**, Snowden et al., 1991; Qian and Andersen, 1994) M.m.*	Suppressed	Suppressed (Snowden et al., 1991; Qian and Andersen, 1994) M.m.*
Speed selectivity	0 (simple cell) 9/33 (complex cell) (**DS**, Priebe et al., 2006) M.m.	3/68	28/104 (Priebe et al., 2003) M.m.
Optimal SF (cycle/degree)	1.5~6 (**DS**, Hawken et al., 1988) M.m.+V.m. 2.4 (mean, **Layer4B**, Jones et al., 2001) M.m. 1.9 (mean, **complex DS**, Bair and Movshon, 2004) M.m.	2.16 (mean)	**~1** (**eccentricity =0~5**, Miura et al., 2014) M.m. 0.9 (mean, Bair and Movshon, 2004) M.m.
Optimal TF (Hz)	7.8 (mean, **complex DS**, Bair and Movshon, 2004) M.m.	8.29 (mean)	**~10** (**eccentricity =0~5**, Miura et al., 2014) M.m.* 11.5 (mean, Bair and Movshon, 2004) M.m.
Optimal speed (deg/sec)	4.47 (geometric mean, **DS**, Priebe et al., 2006) M.m.	4.72 (mean)	**~10** (**eccentricity =0~5**, Miura et al., 2014) M.m.* 32 (peak, Maunsell and Van Essen, 1983) M.m. 32 (peak, Mikami et al., 1986 I) M.m.* 7.52 (geometric mean, Priebe et al., 2006) M.m.
Direction tuning bandwidth ($^{\circ}$)	70 (mean, **complex DS**, Bair and Movshon, 2004) M.m. 14.5 (median, half-bandwidth, **DS**, Gur et al., 2005) M.m.*	76.7 (mean)	91 (mean, Albright , 1984) M.m. 105 (mean, Born, 2000) O.m. 98 (mean, Bair and Movshon, 2004) M.m.
Response latency (ms)	63.8 (mean, **Layer 4B**, Nowak et al., 1995) M.m.	65.5 (mean)	87 (mean, Raiguel et al., 1999) M.m. 68.1 (**Pattern**), 61.8 (**Component**), 62.3 (**Unclassed**) (mean, Smith et al., 2005) M.m.

M.m.: Macaque monkeys; V.m.: Vervet monkeys; O.m.: Owl monkeys; *: Awake;